UNIVERSITY OF OKLAHOMA

GRADUATE COLLEGE

INTEGRATED 3D PRINTING OF ROBOTIC STRUCTURES AND CIRCUITS

A THESIS

SUBMITTED TO THE GRADUATE FACULTY

in partial fulfillment of the requirements for the

Degree of

MASTER OF SCIENCE

By

SEAN S. MCDONOUGH
Norman, Oklahoma
2016

INTEGRATED 3D PRINTING OF ROBOTIC STRUCTURES AND CIRCUITS

A THESIS APPROVED FOR THE
SCHOOL OF ELECTRICAL AND COMPUTER ENGINEERING

BY

_____
Dr. Andrew H. Fagg, Co-Chair

_____
Dr. Sesh Commuri, Chair

_____
Dr. Hjalti Sigmarsson

Acknowledgments

I would like to take thank all those who supped supported me while I worked on my masterғʟs thesis. From family, both those related to me and my Life.Church family in Moore, who has always encouraged me and pushed me to do my best, to friends who were there for the fun time and the not so fun times, to colleagues who have a better understanding of the difficulties involved in graduate school.

I would like to thank my committee members. First, Id like to thank Dr. Andrew H. Fagg. You were my adviser, Co-Chair, advocate and you helped me guide me through many tough challenges. Second, Dr. Hjalti Sigmarsson and Dr. Sesh Commuri thank you for your patient with me through the process and your input into the project. I believe I am a better researcher and engineering because of the experience I gained.

To everyone who let me stay at your house while I finished the last few months of my thesis thank you. I honestly dont know how I would have finished without your generosity.

Lastly I would like to my Lord and Savor Jesus Christ. My faith is an integral part of who I am and I would not have had the fortitude to finish a project of this caliper without it.

Table of Contents

List of Tables

List of Figures

Abstract

Advances in upper limb prostheses have lowered the cost of prosthetic limbs, enabling access for a larger population of amputees. Other advancements, such as robotic prosthetics, enable amputees to more easily grasp objects at will. Some prostheses can even restore the sensation of touch to an amputee. Adding functionality to the prosthetic devices can also increase the price. 3D-printing offers a means to produce prostheses at a lower cost. Work has already been done to create a 3D-printed robotic prosthetics. This thesis presents preliminary research in the direction of a 3D-printed, sensing prosthetic hand. One way of reducing cost and increasing reliability is to print conductive elements into the structural components of prostheses instead inserting or attaching them after fabrication. I use a new conductive PLA plastic, F-Electric ^{TM}, to print the paths for the sensor data to travel. In this thesis, I establish a set of procedures for mixed material printing, in which one of the materials is electrically conductive. I construct several pressure sensors utilizing the conductive material for the electrodes. The sensors nominally perform as expected and can be seen as a step towards a 3D-printed tactile sensing prosthetic hand.

Chapter 1

Introduction

Prosthetic limbs come in many styles with a varying degree of complexity. They can range from simple static replacement limbs to highly complex electronic limbs or myoelectric prostheses. The more advanced prosthetic limbs can respond to inputs from the amputee or even provide feedback. The additional hardware can, for example, allow a prosthetic hand to open and close, restoring the ability to grasp objects with the prostheses.

Designing a prosthetic limb for an amputee requires a high degree of customization. Each prosthesis must be attached to the remaining portion of the amputeeFLs limb in a way that provides both stability and comfort for the individual. The type of prostheses needs to match the desired functionality of the amputee. Grasping objects with a prosthetic hand is not a trivial task. Factors that go into a grasp include the shape, size, surface material, weight and malleability of the object. A high degree of precision is needed for many everyday tasks. For example, buttoning up a shirt requires the individual to grip the small button in one hand and be able to align it

with the hole on the other side of the shirt. Finally, the cost of the prosthesis needs to fit within the budget of the amputee.

A new prosthetic limb, without electronic components, can cost anywhere between $3,000 and $50,000 (Mohney, 2013), depending on the type of prostheses and quality of the product. The high cost is attributed to the customization needed for each individual, as well as the high material cost for parts, such as light weight aluminum. The high-grade materials provide durability while remaining light enough to not encumber an amputee. The additional hardware and complexity of a myoelectric prosthesis can increase the cost up to $100,000 (Gibbard, 2013). The increased cost allows the amputee greater control over grasping ability than a traditional prosthesis. Wita myoelectric prosthesis, an amputee can control grasping function by signals received from their muscles.

Another way to further increase the accuracy of a grasp is to introduce tactile and proprioception feedback. For example, the tactile feedback induced by the prosthesis designed by Tan et al. (2014) allowed subjects to have improved control of their grasping strength, as well as better manipulate delicate objects, such as cherries. One of the challenges involved is long term nerve damage. The nerves are artificially stimulated to create the tactile sensation. It is possible that the method of stimulating the nerve damage the nerve or that the apparatus that delivers the signal could degrade over time causing a reduced sensation. However, one subject used the prosthesis for over two years in the lab without any degradation of feeling. Another challenge of tactile feedback prostheses would be the cost. The increased complexity

and customization needed is likely to be more expensive than a standard myoelectrical prosthesis.

A way to mitigate the high cost of these prosthetic limbs is to utilize 3D-printing. Examples of individuals creating DIY prosthetics include a family friend printing a prosthetic limb for a child born without fingers (Grout and Truesdell, 2014) or a father printing a prosthetic hand for his child (Velez, 2014). Prostheses made through 3D-printing can be cut to a fraction of traditional prostheses mainly because of the lower material cost (Gibbard, 2013). A lower price point opens up the market to many individuals who otherwise would not be able to afford a prosthesis. The cost is so much cheaper that there has been a push for Do-it-Yourself prostheses (Buehler et al., 2015). Each amputee can be involved in the creation process of the prostheses. The amputee can choose aesthetic features that suit their personality and the functional features that best suit their needs.

The Open Hand Project is an example of a project accessible to an individual looking to create their own prostheses (Gibbard, 2013). The Open Hand Project focuses specifically on 3D-printed robotic prosthetic hands. The Dextrus, one of the models available on the site, uses stick-on electrodes to read signals from the amputee's remaining muscles to control the printed hand.

The question is then raised: Is it possible to do something similar with 3D-printing and sensing prostheses? Designing a 3D-prosthetic limb with tactile feedback is not a trivial task. One of the primary goals is to simplify the manufacturing process by printing as much of the components as possible. One of the challenges

is how to transmit signals from the sensors at the surface of the prosthesis to the processing unit.

In this thesis, I explore the approach of printing sensor interfaces (wires or electrodes) into the structural components of the prosthetic limb instead of placing them after the prosthesis is fabricated. Printing the electrodes offers a number of advantages, one of these being reduced fabrication time and complexity. 3D-printed electrodes can be routed from the surface to a central location, making the connection from the sensors to the processor simpler. Another advantage is that the durability of the electrodes could be increased. The printed electrodes would be less exposed inside the prosthesis and take less wear and tear from the environment.

In order to print the electrodes, a conductive filament is needed. Conductive plastic filaments have recently become available. As part of my work, I will examine the feasibility of their use. I will run several experiments to verify qualitatively that the filament functions as the designers specify. After the filament is validated, I will integrate the filament with nonconductive PLA to create a simple circuit. Lastly, I will create pressure sensors utilizing the conductive material. The pressure sensors are preliminary work on components that can be used in a 3D-printed sensing prosthetic hand.

The following chapter includes background information and related works. The resistive properties of the conductive filament are investigated in Chapter 3. The conductive filament is embedded in nonconductive PLA to form a simple circuit in Chapter 4. A sensor utilizing the conductive material is designed and evaluated in Chapter 5.

Chapter 2

Background

2.1 Upper Limb Prostheses

Upper limb prosthesis can be categorized into three main types of prosthesis (Biddiss and Chau, 2007). First, passive prostheses serve only as a replacement limb. Second, body-powered prostheses have additional functionality powered by the remaining portion of an amputated limb or other parts of the body. Hands or specialized hooks can be open or closed depending on the motion of specific muscle groups. Cables are attached to the grasping device on the end of the prosthetic limb. By applying tension to the cable, the amputee can open the grasping device. Releasing the tension closes the grasping device. Third, electric prosthesis (myoelectric) utilize circuitry and motors to improve grasping strength and ability. Electrical prostheses can then be subdivided into two groups: prostheses with and without sensory feedback.

The DEKA Arm is a high-end example of a myoelectric prostheses without sensory feedback (Resnik et al., 2014). The DEKA Arm has three configurations: radial, humeral, and shoulder. The prosthesis has six preprogrammed grip patterns and four

wrist movements, with a total of ten powered degrees of freedom. The prosthesis is controlled through a combination of myoelectrodes, pneumatic bladders, foot controls or other common input devices. The individual can practice with the various methods of control to achieve different types and degrees of motion. The foot sensors utilized microelectromechanical systems (MEMS) accelerometers to detect ankle and foot movements. The arm goes into standby mode automatically when a walking motion was detected. The arm has an embedded wrist display that notifies the user of the operating mode, low battery and other useful information. The DEKA Arm has many advanced features that enable better grasping and an overall increase in quality of life.

2.2   Sensing Prostheses

Work has been done as for many years towards the goal of restoring the sensation of touch to amputees. Clippinger et al. (1974) use single channel nerve cuff electrodes to provide sensory information for the prosthetic hand. A nerve cuff consists of a set of electrodes that are surgically implanted around the outside of a nerve. The cuff surrounds the nerve just as a sleeve of a shirt would surround an arm. The electrodes are stimulated giving the amputee a feel of touch that is located where their hand should be. However, the sensation was in a large area as opposed to the desired stimulation of a specific location on the hand. The sensations also varied for each subject.

Ekman (2016) designed a prototype pressure-sensitive skin. Hammond et al. (2014) developed an embedded glove to track human motion with tactile pressure sensors. The stimulation of the digits is done using phantom mapping. In this, the digit on the prosthetic hand that is stimulated is relayed to the area on the stump which corresponds to the same digit. The sensors used are atmospheric pressure sensors based on MEMS-technology. The sensors have Complementary Metal-Oxide Semi-conductor (CMOS) circuitry hermetically sealed within a hard casing. A piezoresistive element is deflected by changes in pressure, and the information is transported to the integrated component interface. Resistive strain gauges are also used to help determine the location of fingers and to assist with grasping.

Raspopovic et al. (2014) have been doing research in the area of sensor-equipped prosthetic arms. Transversal intrafascicular multichannel electrodes (TIMEs) are connected to the prosthetic hand sensors. TIMEs are similar to the cuff electrodes but utilize more electrode channels. The channels can be stimulated individually, causing the subject to perceive a tactile response located on the missing hand. Figure 2.1a shows the sensory loop for the feedback prosthesis. When pressure information is received by the force sensors on the prosthetic hand, a current is generated to match the perceived pressure. This current stimulates the Median and Ulnar nerves causing the amputee to feel the sensation of touch on a phantom hand. Below S_{15} the subject was not able to perceive a tactile response. Greater than S_{75} caused the subject pain and thus was used as an upper limit. The TIMEs cover the outside of the Median and Ulnar nerves, as seen in Figure 2.1b and Figure 2.1c. The subjects were able to distinguish a round object from a spherical object. They also had the ability to
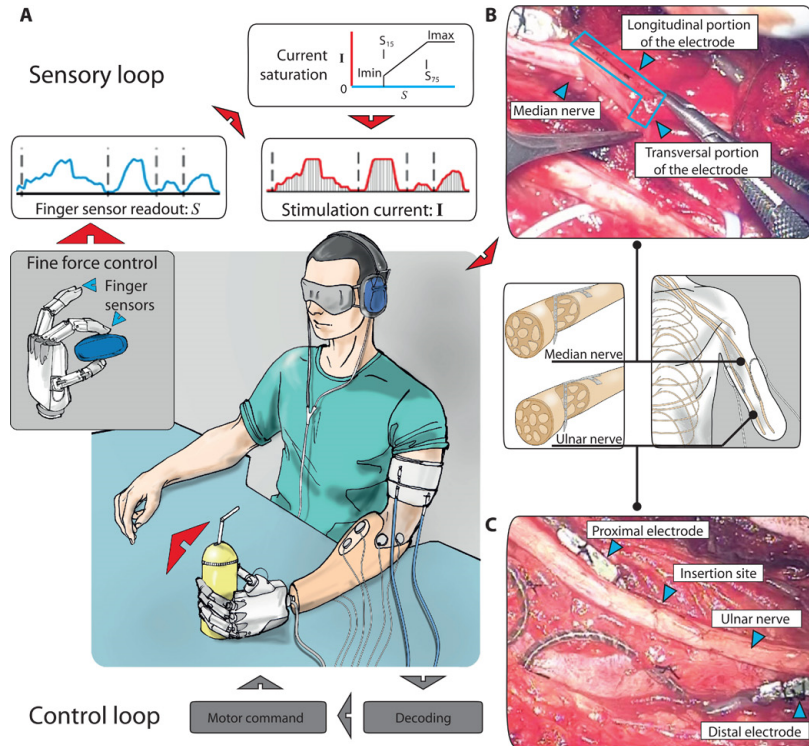
Figure 2.1: (A) Sensing loop with current response. S_{15} and S_{75} are 15 and 75 % of the range of sensor values, respectively. (B) Photo of median nerve during TIME insertion. (C) Photo of ulnar nerve with two implanted electrodes. Adapted with permission from Raspopovic et al. (2014). ©2014 The American Association for the Advancement of Science

control the grasping strength. While the results were promising, the study only lasted 4 weeks. Questions of how the stimulus might affect the amputee in the long run are a concern. It is not known whether the sensation of touch will fade over time due to either degradation in the TIMEs or damage to the nerve.

Tan et al. (2014) have performed long-term experiments with subjects to restore the sensation of touch. Nonpenetrating peripheral nerve cuff electrodes are used to stimulate a phantom hand for the subjects. The electrodes are inserted along the Median, Ulnar, and Radial nerves. Two subjects participated in the research and had access to the prosthetic hands for 16 and 24 months. An experiment was conducted

to demonstrate the functionality of the prostheses. In the experiment, the subject is given the task of removing the stem from cherries while blindfolded. The subject holds the cherries with their prosthetic hand and removes the stem with their intact hand. First, the test is done without the sensing feedback. The subject can tell when the hand is opening and closing but consistently crushes the cherries when obtaining a grasp to remove the stem. When the feedback is turned on the subject was able to grasp the cherries and remove the stems without damaging a majority of the cherries.

2.3   Methods of 3D printing

Three-dimensional (3D) printing is a form of additive manufacturing where an object is created by placing layer after layer on top of each other until the full structure is complete. The first 3D printers used stereolithography (SLA) to print objects (Hull, 1986). Figure 2.2 shows the schematic of an SLA printer. In this method, resin from a reservoir is cured using a laser, thereby creating a single layer. The next layer is added by moving the stage so that another layer of resin can be cured by the laser.
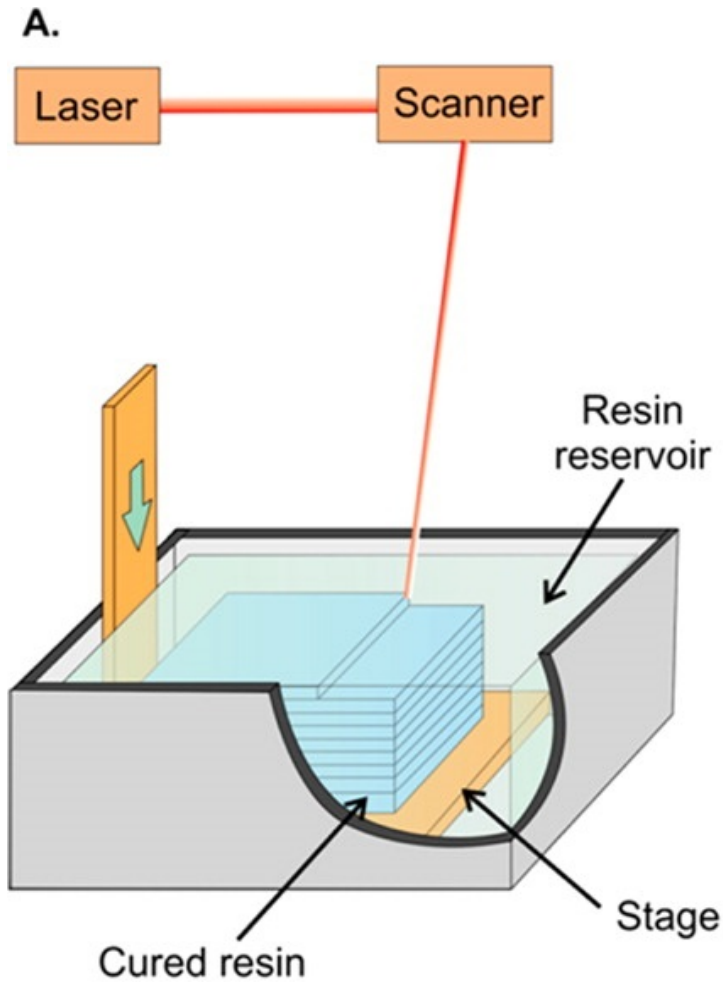
Figure 2.2: (A) Process for bath SLA printer. Adapted with permission from Gross et al. (2014). ©2014 American Chemical Society

Inkjet printing was the next form of 3D printers. Figure 2.3 shows an overview of the process of Inkjet printing. An inkjet printer has a printing stage that is covered with powder. Two methods are used for bonding the layers together. The first method is a liquid binding agent that binds the layers together. The second method is a laser that fuses the layers together. After a layer is finished, the fabrication stage moves
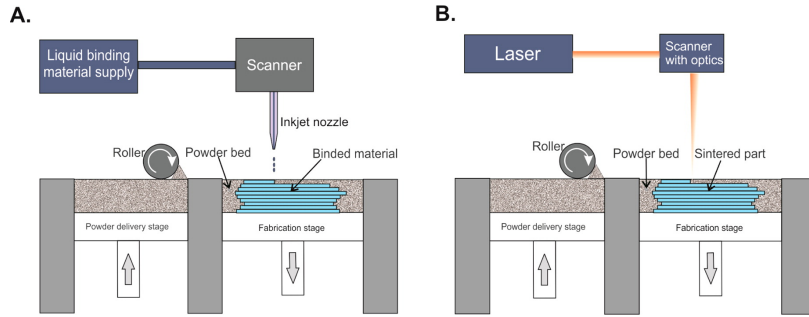
Figure 2.3: (A) Proccedure for a inkjet printer. (B) Diagram of an SLS 3D printer. Procces for embedding electronics into 3D-prints developed Reprinted with permission from Gross et al. (2014). ©2014 American Chemical Society

down, and a new layer of powder is added to the stage. Then the process is repeated untill the model is finished.

As shown in Figure 2.4, in Laminated Object Manufacturing (LOM) a sheet of material is stretched out over a stage (Feygin and Pak, 1999). Either a laser or other cutting apparatus is used to trace out the shape of the object. The layer is then fused to the previous layer by some adhesive or, in the case of metal, welded together. After a layer is complete, the stage is lowered, and the excess sheet of material is rolled away and replaced with a new sheet.
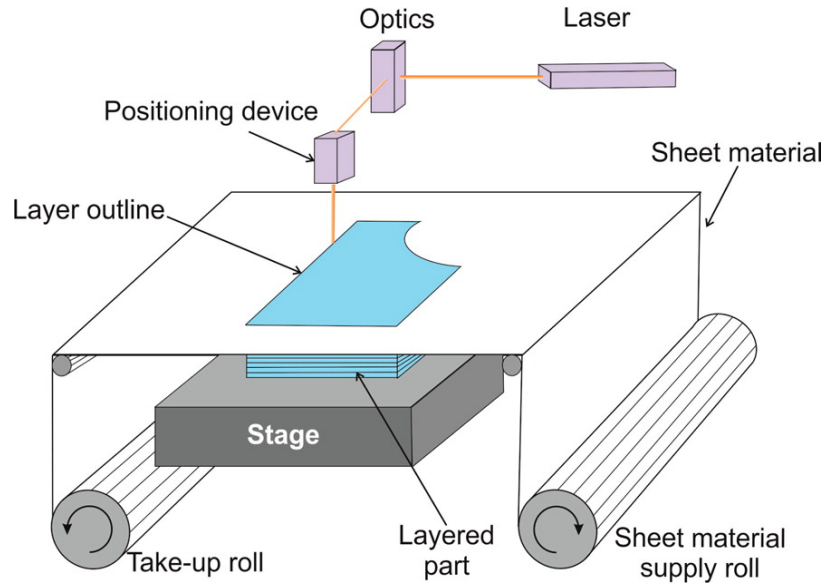
Figure 2.4: Schematic of an LOM 3D printer. Reprinted with permission from Gross et al. (2014). ©2014 American Chemical Society

As shown in Figure 2.5a, Fused Deposition Modeling (FDM) is the process of heating a material to the point of melting then depositing the material into layers to create a 3D object. It is the method of printing used throughout this research project. In FDM a spool of material is fed into a chamber. The filament is pushed through the heated nozzle as the head traces out the 2D design for that cross-sectional layer. The types of material printed can range from paper, nylon, wax, resins, metals and ceramics (Novakova-Marcincinova et al., 2012). There can be a number of different versions of a material that can be printed as well. For example, acrylonitrile butadiene styrene (ABS) and Polylactic acid (PLA) are two common types of thermoplastics available for 3D printing. PLA is generally biodegradable, able to achieve sharper corners and does not warp much after printing (Chilson, 2013). Warping is when the heated material has expanded then begins to contract as it is cooling, losing the

desired shape. However, PLA loses some of its structural qualities if the ambient temperature goes beyond 50° C. ABS is petroleum based, has a higher temperature resistance and is more flexible than PLA. However, it requires a higher printing temperature and is prone to warping. ABS warps more because it contracts more as it cools. A heated print bed is used to reduce the amount of warping that is seen with ABS.

The design of the 3D printer dictates which materials that a particular model can use. The 3D printer used in this research, the MakerBot® Replicator 2X®, is designed to print plastic filaments. Figure 2.5b shows the printed used in this thesis. The printer is modifed slightly to better accomidated PLA printing.
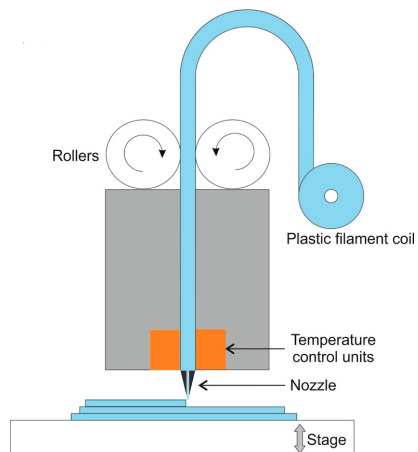
(a) Schematic of a FDM 3D printer
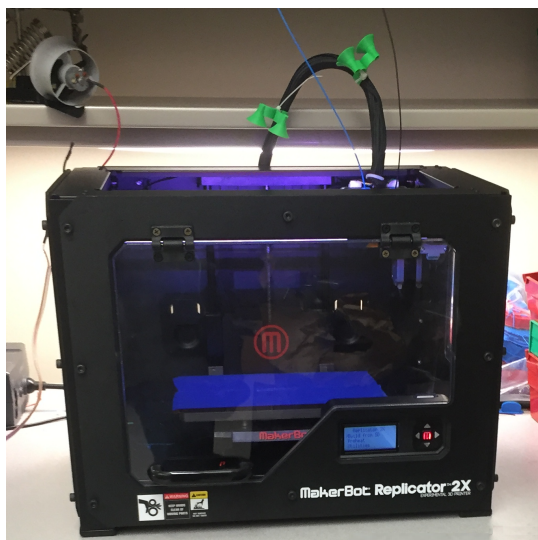
(b) MakerBot® Replicator 2X®

Figure 2.5: (a) Visual representation of FDM printing procces Reprinted with permission from Gross et al. (2014). © 2014 American Chemical Society (b) MakerBot® Replicator 2X®set up for printing PLA.

The slicer is the software that takes the 3D model to be printed and breaks it up into cross-sections for the printer to produce. In particular, it plans the path of the printhead. And determines how the material is to be placed. Three key features in

how the object is going to be printed are the *infill percentage*, *infill design* and *shells parameters*. The slicer will trace out the surface of the volume of the model a number of times equal to the shells parameter. Then the remainder of the space will be filled only to the amount of the infill percentage using the design specified in the infill design. For example with infill percentage equal to 10 percent and an infill shape of hexagons, then only 10 percent of the remaining space between the shell walls would be filled with hexagons.

2.4   DIY Prostheses

Hurst and Tobias (2011) focus on a broader topic of DIY Assistive Technology. Projects include a helmet that allows the user to paint a picture, a custom built miniature wheelchairs and modifications for wheelchairs. While Hurst and Tobias (2011) do not focus on prostheses, the spirit behind the project is the same. Allowing individuals to customize the care they received based on their needs and preferences.

Buehler et al. (2015) explore the 3D models for Assistive Technology on Thingiverse.com. Thingiverse is a site that host open source 3D models (things) for 3D-printing. Prosthetic (44) and prosthesis (17), was second highest of the top 15 keywords of 3D models identified as assistive designs. 41 of the things consisted of prosthetic hands, hooks, and related parts. A majority of the designers had no background in STEM fields. The designs that have been achieved are impressive; however, the question has to be raised of what can be done by a focused engineering effort into the field of DIY prosthetic limbs.

The Open Hand Project is an example of a better-engineered project (Gibbard, 2013). The Dextrus hand is designed to attach to a preexisting prosthesis. Each finger can be actuated individually with dc motors. Feedback tells the processing unit in the hand when an object is being grasped. The feedback allows the hand to grip unusually shaped objects better. The feedback is only given to the processing unit of the hand, not to directly to the individual. Providing feedback to the amputee could be a means of further increasing grasping ability and improving the individuals quality of life.

2.5 3D printed sensors

Manufacturing electronics using 3D printing has been done for a number of years. Shemelya et al. (2013, 2015a,b) look to embed electronics during the printing process to create a printed conductive sensors. The electronics are embed directly inside the model midprint, as seen in the Figure 2.6. The first panel shows the printed model with cavities for the electronics. The second panel has the electronics in place, but not the connecting wires. The third panel has the wires in place. The final panel shows the finished model with electronics fully embedded. The model response to applied pressure over the senor and the embedded LEDs light up.

Hübler et al. (2011) used gravure and flexographic printing to create a vertically stacked ring oscillator. Both printing techniques utilize an master copy that is pressed against the paper to deliver the intended design. Gravure printing utilizes a metal roller, while Flexographic uses flexible resin plates. Their team was able to create
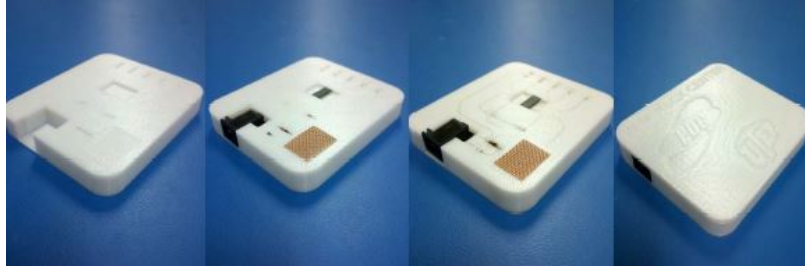
Figure 2.6: Procces for embedding electronics into 3D-prints developed by Shemelya et al. (2013). ©2013, IEEE

the various components of the oscillator using planar printing. After printing, the strips are attached together using conductive tape.

2.6 Conductive Plastics

Leigh et al. (2012) proposed *Carbomorph* a conductive filament. The cited resistivity measurements for Carbomorph are in-plane with the layers as $9.60\,\Omega - cm$ and perpendicular to the layers as $12.60\,\Omega - cm$. The material is piezoresistive and is capacitive. The material changes its resistivity based on the amount the flexion. The capacitance changes based on the amount of pressure applied to the material. The piezoresistivity was highlighted with a single flex sensor and a printed glove with a sensor for each finger. A human interface device (HID) consisting of three buttons highlighted the capacitive capabilities of the material. When one of the buttons was pressed by a finger, the capacitance changed. A mug was also used to show the capacitance of the material. The material would change capacitance based on the amount of liquid in the glass. Both the single flex sensor and the HID had connectors designed specifically for banana plugs. The connectors were designed to allow for

easy connection and testing of the devices. A similar approach was taken for this project to make testing of the printed sensors easier. The major limiting factor for Carbomorph is that it is not commercially available. Leigh et al. (2012) give instructions on how to fabricate the material, however doing so is outside of the intended scope of the project.

Proto-pasta Conductive PLA ^{TM} produces a commercially available conductive PLA (Cram et al., 2015). The conductivity of the material is achieved through the use of electrically conductive graphite. It has a cost of approximately \$30 per half a pound. The resistivity of the material in-plane with the layers is $30.0\,\Omega-cm$ and perpendicular to the layers is $115.0\Omega-cm$. The suggested printing temperature range is 215-230° C. The material is more flexible than PLA but has less layer adhesion.

Functionalize ^{TM} created F-Electric ^{TM}, another conductive filament (Toutonghi, 2015). The conductivity for the material is achieved through the use of carbon nanotubes. The cost per half a pound is \$71. While it can bond with a number of standard filament types, its properties are closest to those of PLA. Toutonghi (2015) claim that the plastic is stronger than traditional PLA and has a better dimensional stability, meaning it will not shrink as much. It has a reported volume resistivity of 0.75 ohm-cm. Toutonghi (2015) advise to keep the printing temperature between 215-230° C. They also advise to print the conductive material along the line current is to flow, to improve the conductivity of the print. A print along the direction current flow allows for the current to travel down a single strand of material. Printing opposed to the direction of current flow means covering multiple layers that are fused together instead of long beads of material.

2.7   Force Sensitive Resistor

In this research, a force sensitive resistor (FSR) fills the job of the sensor. The FSR material consists of a matrix of *carbon_black* suspended in a polymer. As pressure is applied to the material the polymer material compresses and the distance the electrons have to travel through the material at that point is shorter, thus lowering the resistance.

Chapter 3

Quantifying Performance of Conductive Plastic and Successful Practices

Conductive 3D printable filaments have only recently been made commercially available. Because these filaments are printable using semi-professional or hobbyist 3D-printers, one can imagine embedding wires and ultimately circuitry into many different types of 3D-printed devices. These include robots and DIY prostheses. In this chapter, I quantify the performance of a particular conductive plastic and describe a particular set of techniques that can be used with a Makerbot Replicator to print this material effectively.

The first task is to determine which conductive filament is best suited for the end research goals of routing signals away from sensors. While the flexibility offered by Proto-pasta™ might have useful applications in the future, the lower volume resistivity of F-Electric™ makes it more desirable. Having selected a conductive filament, I conduct several experiments to determine if the material matches the characteristics given by Functionalize™.

One major challenge with printing with thermoplastics is establishing an appropriate print temperature. The temperature has to be high enough that when the material comes out of the nozzle, it will fuse to the plastic on the previous layer. However, if the temperature is too high, then the filament can melt prematurely and seep out or become soft as it enters the print head and clogs the nozzle. A conductive filament increases the complexity of the process. Now, in additional to needing to bond to the material already printed, the question arises of whether the conductivity is preserved at that temperature. Functionalize™ gives a suggested temperature to print the plastic. Does the resistance of the material after printing match the theoretical values calculated from the given resistivity?

Toutonghi (2015) also advised that the print head should travel along the direction electrical current is supposed to flow. What are the implications of printing direction against the desired direction of current flow? Are there other, more general, effects that printing direction can have on the outcome of a print?

In this chapter, I look to determine if the material matches the expected volume resistivity. In addition, I will develop some practices that help maximize the chance of a successful print.

3.1   Material Verification

F-Electric ™ can be used to fill many of the roles that traditional wires typically hold. If F-Electric ™ is to take the place of wires, several factors must be taken into consideration. Traditional wiring has a minimal resistance value. The presence of

Figure 3.1: Profile of a $4\ mm \times 4\ mm \times 30\ mm$ sample. The additional material at the ends of the material is used to mount the piece in the testing apparatus.

resistance in the lines can fundamentally change circuits. It is thus important that the conductive material have a low resistance after printing. Other factors, such as thermal properties of the material after printing, are important as well.

3.1.1 Resistive Property

The published volume resistivity of the material is $0.75\Omega - cm$ (Toutonghi, 2015). Given that, resistance is related to resistivity by:

$$R = \frac{\rho\, L}{A} + r_c, \tag{3.1}$$

where ρ is the volume resistivity, L is the length of the sample, A is the cross-sectional area of the sample, and r_c is the contact resistance. According to Equation 3.1, for a given length, the resistance of a sample will increase as the cross-sectional area decreases. Conversely, for a given cross-sectional area, the resistance of a sample will increase as the length increases.

In order to test the accuracy of the reported value, an experiment was conducted using varying lengths and cross-section areas of the material. The resistance of each printed model was compared with the theoretical value calculated from the given resistivity and the dimensions of the sample.

The correlation of cross-sectional area and length to resistance is used as a guide for five sets of printed samples. In three of the cases, the cross-sectional area is held constant while the length varies. There should be a linear relationship between the length and the resistance of a sample. In three of the cases, the length is held constant while the cross-sectional area changes. There should be an inverse square relationship between the recorded resistance and the cross-sectional area. The middle case will be shared between the two experiments.

Figure 3.1 shows the CAD model of one of the samples. The design consists of rectangular prisms with brackets on the ends to make sure that each sample is mounted consistently. The brackets are used to ensure the same orientation of each sample during the measurement process. All samples are printed with ten percent infill and five shells. Using five shells is a way to ensure that the larger samples will be completely filled, without having to change the infill amount. The shells are set to a size of $0.4 \ mm$. Keeping the end goal of integration with a prosthetic hand in mind, the values chosen for the samples can fit a number of joints in an adult hand (Alexander and Viktor, 2010). For three of the sets of samples, the cross-sectional area is held constant at $3 \ mm \times 3 \ mm$ with lengths of $30 \ mm$, $45 \ mm$, and $60 \ mm$. For three sets, the length was held constant at $30 \ mm$, while cross-sectional region was one of $2.4 \ mm \times 2.4 \ mm$, $3 \ mm \times 3 \ mm$, and $4 \ mm \times 4 \ mm$.

A cross-sectional area of $2.4 \ mm \times 2.4 \ mm$ was chosen over $2 \ mm \times 2 \ mm$ because, in the latter case, an empty channel, as seen in Figure 3.2a, was present in the middle of the print. This means that the actual cross-sectional area is smaller than desired. The channel in the middle is smaller than the size of the material coming out

23

(a) $2\ mm \times 2\ mm \times 30\ mm$ with gap

(b) $2.4\ mm \times 2.4\ mm \times 30\ mm$ with gap
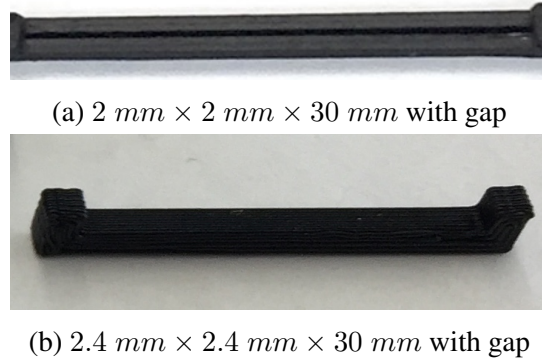
Figure 3.2: Side by side comparison of $2\ mm \times 2\ mm \times 30\ mm$ printed sample and $2.4\ mm \times 2.4\ mm \times 30\ mm$ printed sample.

of the nozzle. As a result, the slicer does not attempt to place a bead at this location.

A sample with the cross-sectional area of $2.4\ mm \times 2.4\ mm$ does not have the gap

in the middle, as seen in Figure 3.2b, and thus is used for the experiments.

Screw terminals were used to hold each sample during resistance measurements.

The screw terminals provide enough surface area of contact to obtain a stable mea-

surement. Before employing screw terminals, both leads from an ohmmeter and

alligator clips were used with little success in obtaining a stable measurement. The

resistance readings from either source fluctuated greatly.

Figure 3.3 shows a sample mounted for measurement inside of the screw ter-

minals. The terminals gave a consistent reading for the samples. The tin plated

aluminum screw terminals are conductive and thus had a minimal effect on the mea-

surements being made. The contact resistance, the resistance added by the screw

terminals, will be determined using the results from the length test.

The hypothesized reason for the difficulties in measurements is due to the surface-

area of the connection between the printed filament and the metallic conductor. A

larger surface area allows for greater contact between carbon nanotubes responsible

Figure 3.3: *Screw terminals used to in conjunction with an ohmmeter to obtain resistance values of samples. Each side is connected to one of the leads coming from the ohmmeter.*

for the conductivity of the material and the conductor attaching the printed piece to the rest of the circuit. This topic is addressed in more detail in the next chapter.

3.1.2   200° C Print Temperature

Toutonghi (2015) gives the optimal temperature for printing with F-Electric ™ as 215-230° C, as compared to normal PLA range of 180- 220° C (English, 2012). However, the conductive filament fails to load at the higher temperature range. The end of the filament becomes malleable, and the teeth on the extruder cannot grip the filament. The filament was able to load and print at a lower temperature of 200° C.

Ten samples of each set of dimension were printed at 200° C. The resistance of each sample was measured using the aforementioned process involving the screw terminals. Figure 3.4 shows box plots of the resistances measured during the length and cross-sectional area tests. The length test shows the resistance increasing linearly as the length increases. The cross-sectional area test shows an inverse square relationship between the resistance and the cross-sectional region. Both tests fit the expected relationship between resistance and the dimensions of the printed piece. However, the measured values are an order of magnitude away from the expected values. The

measured resistances have a range of approximately 140 - 500 Ω instead of the expected resistances value range of 14 - 50 Ω. A larger analysis of the data was deemed unnecessary because of the large amount of error in the measured resistance values.

Toutonghi (2015) gives the optimal temperature for printing with F-Electric [TM] as 215-230° C. The printing temperature was set to the lower value of 200° C because the current procedure for operating the printer would not allow for higher temperatures. However, if the material is not meeting the designated resistivity at this lower printing temperature, then either the material is faulty, or a change is needed in the printing process to properly utilize the material. I hypothesize that a change in the printing process will allow a higher temperature to be achieved.

3.1.3   230° C Print Temperature

I found that a change in the process for loading the conductive filament enables a higher print temperature. Previously the pre-heat setting was a limiting factor. Normally, this temperature is set at the same value as the desired printing temperature. Once activated, the preheat feature warms the nozzles to the specified temperature. After this temperature is reached, the nozzles can be loaded with filaments. However, at 230° C, the filament melts before it can be properly loaded into the extruded. Setting the pre-heat temperature to a lower value enables the filament to be loaded properly. After the filament is loaded, the print can start, and the temperature of the nozzle rises to 230° C.
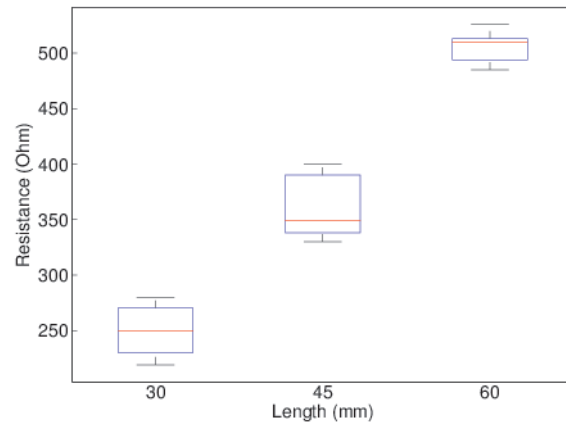
(a) Resistance as a Function of Sample Length
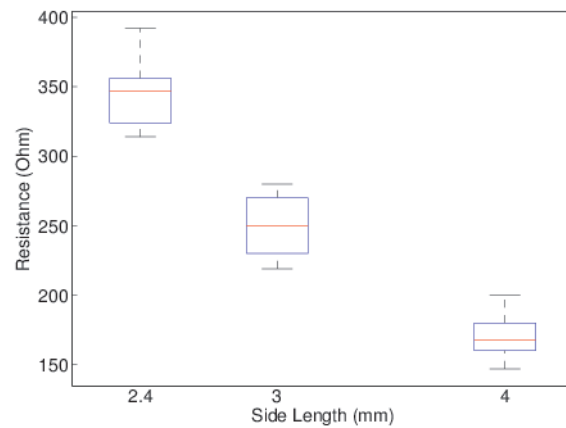
(b) Resistance as a Function of Sample Width

Figure 3.4: Results from the resistance tests. Sample size n = 10. Red lines are the median of the sample set. The blue boxes are the interquartile range. The black hash marks show the range of the samples.

Model Size	Actual Size Range	Expected Resistance
$2.4 \times 2.4 \times 30$	$2.31 - 2.35 \times 2.18 - 2.21 \times 29.96 - 30.07$	44.0
$3 \times 3 \times 30$	$3.13 - 3.18 \times 3.08 - 3.09 \times 29.77 - 30.01$	23.0
$4 \times 4 \times 30$	$4.02 - 4.12 \times 4.01 - 4.03 \times 29.79 - 29.81$	13.7
$3 \times 3 \times 45$	$3.18 - 3.23 \times 3.08 - 3.12 \times 44.73 - 45.02$	33.9
$3 \times 3 \times 60$	$3.24 - 3.31 \times 3.08 - 3.12 \times 59.57 - 59.72$	44.1

Table 3.1: Model and Actual Dimensions for 230° C prints. Expected resistance calculated using the average of the actual size range. Units for Model Size and Actual Size: ($mm \times mm \times mm$). Units for Expected Resistance: (Ω)

A reprint of the samples printed at 200° C was conducted at the higher print temperature. In total each sample was reprinted five times. A caliper was used to measure the actual dimensions achieved by each printed sample. The results from measuring the dimensions of the samples can be seen in Table 3.1. The range of values found is given for each sample set. The samples had at most 3.2 % difference in size from one sample to the next for any given set, but most were closer to 1.3 %.

Figure 3.5 shows the measured and expected values for the higher temperature prints. The resistance readings of the samples printed at 230° C were deviated from the theoretical values by between 3-30%. The measured values approximately fit the expected trends for both the length and cross-sectional area tests. The trend line for the length test had a root mean square error of 1.457 Ω. The cross-sectional area trend line had a root mean square error of 2.742 Ω.

The contact resistance of the screw terminals was found to be a negative 6.3 Ω. The contact resistance was found by determining the y-intercept of the trend line. Though the values is negative, this is not unhearded of when using carbon nanontubes (Nouchi et al., 2012). Another factor is that the sample size used in determining

the trend line is low. At lower a sample size the generation of a trend line is more susceptible to noise.

Based on the result from the prints at varying temperatures, it appears that if the temperature of the nozzle is not hot enough, then the connections between the conductive elements in the filament will not be properly formed. The results for the higher temperature prints are consistent with the published resistivity of the F-Electric ™ material. The experiments highlight the importance of having the proper settings in place for a successful print.

3.1.4 Direction of Print and Current Flow

In the previous section, it was shown that the print temperature is vital to creating the proper connection between the carbon nanotubes. It is hypothesized that a similar effect is seen when printing along the desired direction current is to flow. When the print head travels along the direction current will flow, the layers form as longer lines of material, as seen in Figure 3.6a. In this case, the current flows along the long lines from one end to the other. Conversely, in a print perpendicular to the desired direction of current flow, many layers are smaller and stacked up side by side, as seen in Figure 3.6b. In this case, the current has to flow from one layer to the next to get through the printed wire. If the layers are not fused properly, then I expect a much higher resistance for the vertically oriented print

Two sets of prints are made to verify the hypothesis that it is better to print along the direction of current flow. Figure 3.7a shows an example from each of the sets.
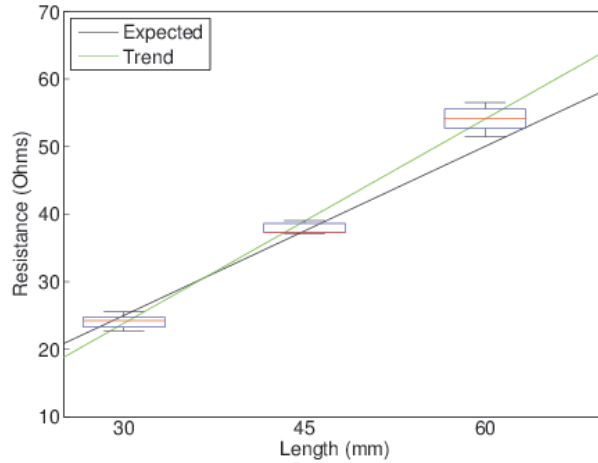
(a) Resistance as a Function of Sample Length
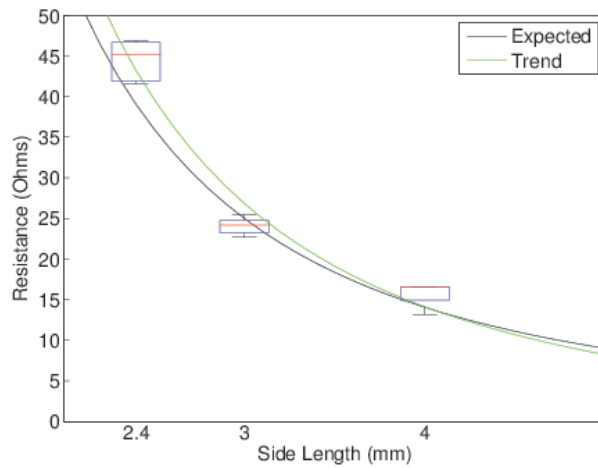
(b) Resistance as a Function of Sample Width

Figure 3.5: Results from the resistance tests. Sample size n = 5. Blue, red and black whiskers in the box plot represent the inter quartile range, the median value, and the range of the samples, respectively. The black lines represent the expected values. The green lines represent the projected trend line of the sample. (a) Resistance values for lengths of $30\ mm$, $45\ mm$, and $60\ mm$. (b) Resistance values for side lengths of $2.4\ mm$, $3\ mm$, and $4\ mm$
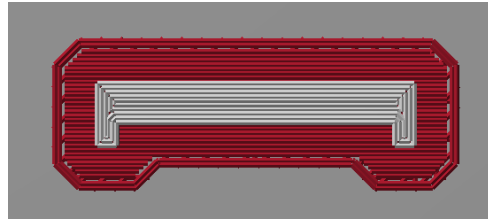
(a) Horizontal print. The white layers of material are longer and run from one end of the print to the other.
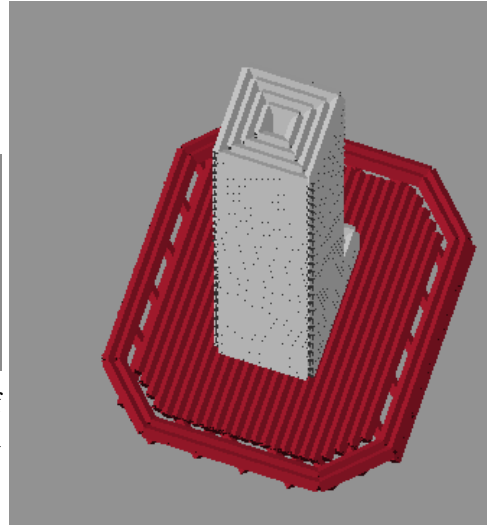
(b) Vertical print. The white layers of material are smaller and are built up from the bottom to the top.

Figure 3.6: Two samples show the classifications for prints. The red material is used for a base raft while the white is the material used for the part.

The dimensions of the sets to be printed are $4\ mm \times 4\ mm \times 30\ mm$. The samples for the horizontal portion of the experiment are the same $4\ mm \times 4\ mm \times 30\ mm$ samples as for the previous section. Structural consistency was the deciding factor for the dimensions of the samples for this experiment. Cross sections smaller than $4\ mm \times 4\ mm$ could not be used for the vertical prints. Vertical prints for prisms with the cross sections of $2.4\ mm \times 2.4\ mm$ and $3\ mm \times 3\ mm$ failed to retain the desired shape. Part of the reason behind this is the fact that the plastic is still malleable for a time after it comes out of the nozzle. The nozzle can also collide with the existing material as it travels, moving the already printed material slightly. The next bead of material is then printed incorrectly, and the shape of the object is distorted, as seen in Figure 3.7b.

(a) Horizontal vs vertical print test.

(b) Example of a vertical print with cross-sectional area of $2.4mm x 2.4mm$.

Figure 3.7: (a) The vertical sample is on top and the horizontal on the bottom. (b) A vertical print that failed to maintain the desired shape of a rectangular prism.
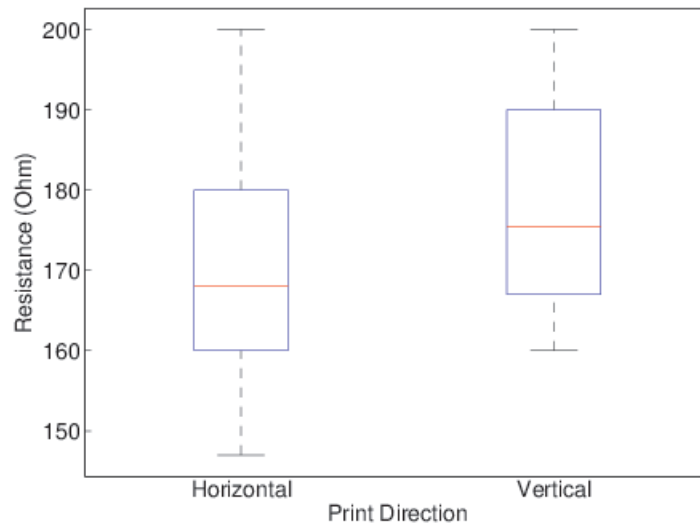
Figure 3.8: $4mm \times 4mm \times 30mm$ prisms. Red lines denote median values. The blue boxes show the interquartile range. The black hash marks show the minimum and maximum values for the set.

Similar to the last section, an entire round of prints was conducted at 200° C. This round of prints was done at the same time as the prints for the previous section, before the error in resistances was noted. A second smaller batch followed at 230° C. The expected resistance reading for a $4\ mm \times 4\ mm \times 30\ mm$ sample is 14 Ω. Figure 3.8 shows the resistances for the two sets printed at 200° C. The vertical samples measured resistances range from 160 Ω to 200 Ω. The horizontal samples measured resistances range from 150 Ω to 200 Ω. Interestingly the resistances for the two cases are very similar with a large portion of overlap. One expects the vertical case have higher resistance because there is additional nonconductive plastic between the layers of the conductive filament. The 230° C print did see a difference in horizontal

and vertical printing with resistance values of 29 Ω and 47 Ω, respectively. Using the values recorded the resistivity perpendicular to the layers is 1.62 times the resistivity in-plane with the layers. This is higher than Carbomorph at 1.31 but lower than that of Proto-pasta Conductive PLA ^{TM} at 3.83. This means that F-Electric ^{TM} has better cross-layer bonding than Proto-pasta Conductive PLA ^{TM}, but slightly worse than Carbomorph.

The results of this experiment are quite telling. Printing at a lower temperature showed little to no difference in vertical and horizontal printing. The prints done at the higher temperature showed the vertical print having a higher resistance than that of the horizontal. The results from the lower temperature print highlight the importance of proper printing settings. The likely explanation as to why there is little difference between the vertical and horizontal prints has to do with the carbon nanotubes. I hypothesize that at the lower temperate the conductive material is not melting enough to making a good enough bond to conduct properly. In this case, improperly conducting across the layers is roughly the same as improperly conducting along a single line of material. The results of the higher temperature print confirm the assertion that printing along the direction of current flow is desirable.

3.2   Successful Printing Practices

Through the process of printing numerous samples, some practices that lead to a more successful print were found. One observation of the printing process is that the horizontal printing gives a more consistent print than the vertical printing. Horizontal

prints better matched the desired model geometry after printing. The greater accuracy is attributed to the fact that the vertical prints did not have enough time to settle and solidify before the next layer was added. Most of these negative effects can be eliminated in dual printing by the addition of a second plastic that acts as a structural material and helps the piece to maintain the intended shape.

Another important observation is that while the F-Electric ™ filament needs to be printed at 230° C, it must be loaded into the nozzle at a lower temperature. While the higher temperature gives the best results for proper resistance readings, it is too high to load the filament into the extruder. At this higher temperature, the end of the filament melts before it can get pushed through the nozzle, causing a jam. The jamming effect was part of the reason a lower temperature was attempted. Pre-heating the nozzle to 210° C allows the material to be properly loaded. After the material is loaded, the print can be started at which point the temperature is raised to 230° C. The higher printing temperature does, however, mean that if the filament breaks off of the spool mid-print, then the entire print has to be redone. If one is present when the filament breaks during a lower temperature print, then the print can be paused while the filament is replaced. At 230° C, even if the print is paused, the filament cannot be reloaded because it melts before it begins to extrude. The temperature of the print head cannot be changed during a print, else wise the temperature could be lowered to load in the filament after a break.

In this chapter, I confirmed that the F-Electric ™ material acts according to the specifications given by the manufacturer. In addition, I established several practices that will help maximize the chances of a successful print. Two main lessons were

learned from this portion of the research. First, the temperature of a print is vital to creating the proper conductive bond. Second, making a proper electrical connection with the material is vital.

Chapter 4

Embedding Conductive Elements into 3D Printed Structures

In the previous chapter, I determined some practices that improve the chance of a successful print when using F-Electric ^{TM} and verified that it functions as expected. The next step is to embed the conductive filament into 3D-printed structures. There are two fundamental design questions to be investigated. The first question is: how to connect the 3D-printed conductor with a metallic conductor? The conductive material works as the wiring for the printed portion of a model, but the wires need a way to interface with the rest of the circuit. Holes will be printed into the conductive material to mate to the metallic conductors. The holes need to be large enough to fit the metal conductor, but also small enough to ensure the necessary connections. Both mechanical and electrical connections are needed to join the printed components with an outside conductor. To form a mechanical connection there needs to be enough friction between the conductor and the printed filament to keep the conductor in place. If there is not enough friction, then a bonding agent is needed. However,

the bonding agent must also be conductive so that the electrical connections are made to complete the desired circuit. The second fundamental design question is: How to keep printed wires isolated from each other? Bleed-over from one wire to the other will cause a short circuit. A portion of the design work included the practical need to be able to perform experiments on the printed components. To achieve this, I designed the components to mate with a breadboard. This design constraint provided some limitation for the placement of the ends of the electrodes, but due to the nature of 3D-printing, does not limit where the electrodes will end up in the model.

In this chapter, I set up an experiment to determine the smallest hole size that will fit a row header. This experiment is done to find the maximum attainable surface area of the connection between the conductive filament and attaching conductor. I conduct a s econd experiment to determine the minimum achievable distance between two isolated adjacent electrodes. Lastly, I utilize the results from the previous chapter and these two experiments to create a simple circuit.

4.1   Connecting to the Electrodes

The previous chapter showed the importance of surface area on making a proper connection to the F-Electric ^{TM} material. The interface with an electrode is critical for making sure that current is transferred when desired. To facilitate the meeting of the circuit with a standard breadboard, row headers with a diameter of $0.64\ mm$ are connected to the printed electrodes.

The size of a hole in the printed electrodes is needed to be the correct dimensions to attach the row headers. The holes need to be large enough to fit the row header, but small enough to create enough friction to hold the header in place and to maximize the surface area of the contact. Conductive paint is used to cement the row headers in place, creating a semi-permanent bond. It is also important to know the smallest possible hole size for future work. Other metallic conductors can be used with the conductive filaments. Not, all will have the same radius as the row headers. Knowing the available size of holes would enable an easier selection of alternative metallic conductors.

I print several electrodes with holes of varying sizes as an experiment to find the optimal hole size. A successful print is defined as an electrode where there is no excess material and no warping of the shape of the hole.

A test block containing a range of hole sizes is printed. The radii of the holes range from $0.2\ mm$ to $0.8\ mm$ in increments of $0.1\ mm$, with an additional radius of $0.75\ mm$. Figure 4.1a shows the CAD model of the test block. The model was oriented so that the electrodes would be printed horizontally.

Figure 4.1b. The values of $0.75\ mm$ and of $0.8\ mm$ were the only radii tested that were successful for both of the test prints. The quality of the holes diminished as the size decreases. Specifically, the shape of the holes becomes more deformed, and the holes are filled in more than desired. To minimize the size of the hole, $0.75\ mm$ is selected for the remainder of the row header connections throughout this thesis.
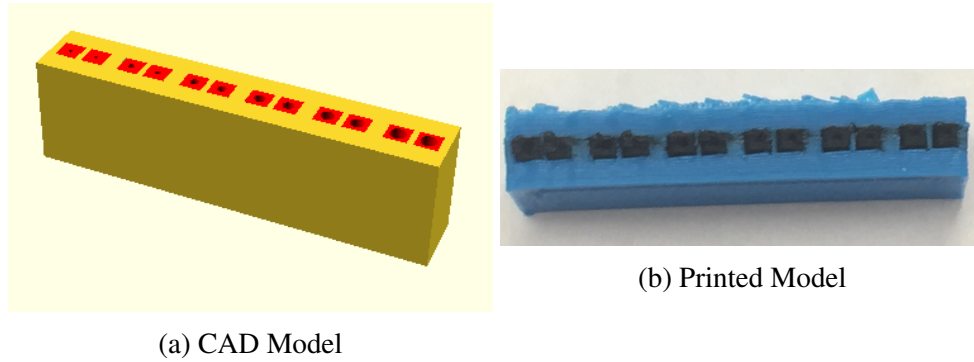
(a) CAD Model

(b) Printed Model

Figure 4.1: (a) Model of radius test from size $0.2\ mm$ to $0.7\ mm$. Red material is conductive. (b) Printed model of radius test. Black material is conductive.

4.2 Isolation of Conductors

3D printing with two materials adds a nontrivial amount of complexity to the fabrication process. The model of printer used was a Makerbot Replicator 2X ™, with dual-extruders. The printing process starts with two test beads at the front of the build plate. If rafting and purge walls are set in the options, those are printed next. The dimensions of the rafting and the purge wall options are automatically determined based on the dimensions of the object being printed.

The printer is set to lay a raft base down so that the print is level and better able to stick to the build plate. The printing of a raft base starts off with a large bead of material that is more likely to adhere to the build plate. After the initial layer, a second smaller layer is printed diagonally across what is already down. Finally, a couple of layers are printed on top of the diagonal layer to create a solid base for the print. The cube in Figure 4.2 is printed on top of a raft base.

Throughout the entire print, the purge walls are added around the edge of where the model will rest. As with the raft base, a purge wall starts with a larger bead to

stick to the build plate. After the first layer, the purge wall consists of two structural towers connected via an L-shaped wall, as seen in Figure 4.2. As each successive layer of the model is printed, an additional layer is added to the purge wall, as well. The purpose of the walls is to allow the material to start flowing from the appropriate nozzle before it is used to print the actual piece. The purge walls also have the additional advantage of catching any material that might still be coming out of the nozzle that is no longer in use.

For each layer of the model, one nozzle prints a layer of the purge wall and the portion of that layer that consists of the current material. Then, the other nozzle prints a layer of the purge wall and fills in the remainder of that layer of the model. After both nozzles have finished a layer, the build platform is lowered, and the process is repeated. Without the purge wall, material from the nozzle may not start to flow until part way through printing the layer. Additionally, material from the other nozzle may also continue to flow for a short while and contaminate the current layer.

The disadvantage of a purge wall is that it adds time and material to the build process. A test was conducted to see the plausibility of printing without a purge wall. If it were possible to print without the purge wall, the cost and production time would be reduced.

To test if it is possible to print without a purge wall and find a minimum distance between two adjunct electrodes, models with embedded wires are printed both with and without the purge walls. The models for the experiment consist of three electrodes printed a variable distance between the centers of the electrodes. A set of preliminary models was printed to find the distances most likely to succeed. The
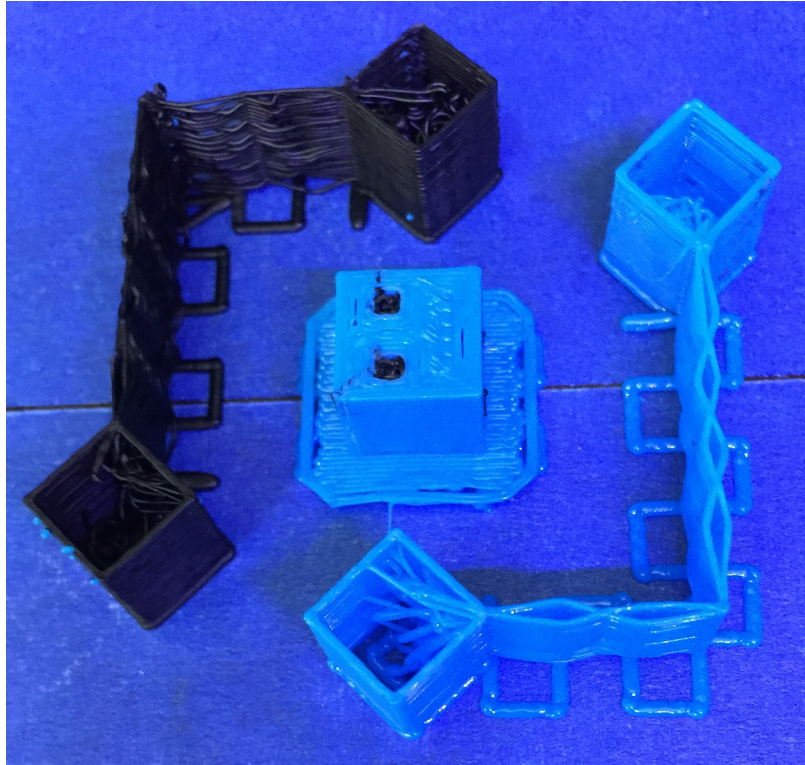
Figure 4.2: Dual material 3D printed object with purge walls around the edge.

distance between the center of the electrodes for both cases starts at $2.54\ mm$, or one electrode per slot in a breadboard, then is incremented by $2.54\ mm$ up to a distance of $5.08\ mm$ with a purge wall and $10.16\ mm$ without the purge wall.

A print is deemed successful if there is no short circuit due to bleed-over between the electrodes. An ohmmeter is used to check if there is conductivity between the conductors.

Figure 4.3(a) and Figure 4.3(b) show an example of an unsuccessful print and successful print, respectively. In the unsuccessful print, the black conductive material can be seen connecting the electrodes that are supposed to be isolated. In addition, the surface should be flush with the edge of the print. In the successful print, the
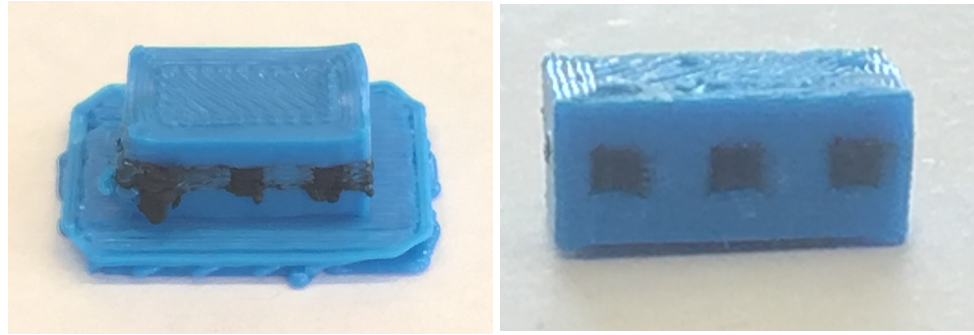
<div align="center">(a) Unsuccessful Print   (b) Successful Print</div>

Figure 4.3: Comparison of an unsuccessful and a successful print. The blue material is normal PLA. The black material is conductive.

conductive material is flush with the rest of the print, and there are no connecting lines between the electrodes.

Twice the header separation distance, $5.08\ mm$, was needed for prints with the purge wall. Seven prints were printed with a purge wall. The success rate with a purge wall was five out of seven or 71.4 %. Four times the separation distance, $10.16\ mm$, was needed for prints without a purge wall. Two models were printed for $10.16\ mm$. Both were successful. However, due to the larger distance needed for a successful print without the purge wall, it was deemed infeasible.

While the purge wall helps to mitigate the bleed-over issues, there are still some cases when bleed-over does occur. It is likely that the bleed-over is caused by the issue of material seeping out of the nozzle after the desired portion is finished. A possible solution is to change the *retraction distance* or *retraction speed* for the nozzle with conductive material. After a section is finished printing, the filament is pulled into the nozzle at the speed and distance specified by retraction speed and the retraction distance parameters, respectively. It is hypothesized that by retracting

more of the filament at a quicker speed, the filament would be farther away from the heating element and bleed-over would be less likely to occur. However, increasing the retraction distance and speed could also increase the risk of the nozzle getting clogged.

4.3   LED Stairs

Having established a protocol for integrating prints with a breadboard, a simple demonstration of the capabilities of the conductive material is shown. A staircase was chosen as the model to demonstrate the versatility of a 3D printer. Each successive step uses a larger amount of the conductive material for the wires inside the structural material. Two electrodes are located on each level, one for the positive lead of an LED and one for the negative lead. Figure 4.4a shows a CAD model of the stairs. Figure 4.4b shows a printed model inserted into a breadboard with the LEDs activated. Using the conductive material simplifies the design of the staircase. Creating a similar model without the conductive material would require physical wires to be fed through open channels. While this is easy with this particular model, more complicated models that include turns in the channels would be much harder to feed.

Several iterations had to be attempted before the final model was printed. Figure 4.4 shows the CAD model for the final printed staircase. The major problem was bleed-over from one electrode to the other on a given step. In the previous section, I determined that a distance of $5.08\ mm$ is needed to maintain isolation of the electrodes. However, the desired size of the staircase would not accommodate two
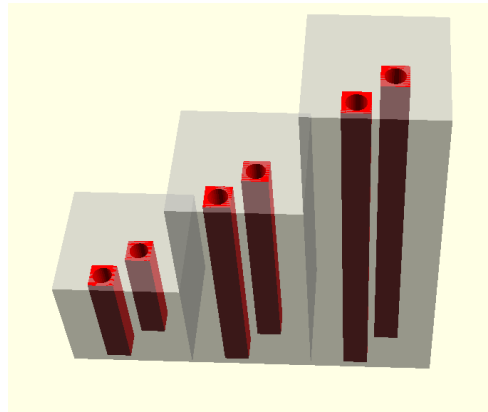
(a) CAD Model. The red material is conductive. The transparent material is normal PLA.
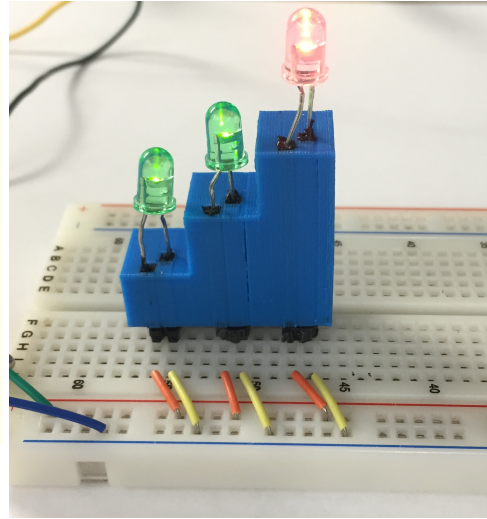
(b) Printed Mode. LEDs are inserted into the conductive material on each step.

Figure 4.4: Three stairs starting at $10\ mm$ in height and increasing to $20\ mm$ and $30\ mm$ with electrodes for an LED through each stair.

electrodes on each step. To work around this limitation, the electrodes are positioned diagonally from one another. The electrodes are printed diagonal from one another, or moved $2.54\ mm$ along the length of the model and $2.54\ mm$ along the width of the model. With electrodes positioned diagonal to each other, each electrode is printed at a different time than the adjacent electrode. Since the electrodes are printed at separate stages in the printing process there is a minimal chance of bleed-over, thus the electrodes can be closer than the minimum distance I determined earlier. This solution gives an option for more compact electrodes, but only applies to electrodes printed at different times.

I answered several questions in this chapter. First, I found an acceptable way to attach conductive elements to the printed electrodes. Second, I determined the

minimum printing distance to maintain isolated electrodes, both for diagonal electrodes, as well as, ones on the same plane. Finally, I showed a simple example of the capability of a 3D-printed circuit.

Chapter 5

A 3D-Printed Embedded Pressure Sensor

In the previous chapter, I successfully integrated the conductive material with nonconductive PLA plastic. This chapter focuses on creating a pressure sensor that utilizes 3D-printing. The sensors are meant to be the first stage in designing a 3D-printed, tactile-sensing prosthetic hand. One of the challenges with creating a tactile sensing prosthetic hand is delivering the wires from the base of the hand to the sensor on the surface. I aim to provide a solution to this problem using the conductive filament F-Electric ^{TM} as the wires that deliver the sensory information to the rest of the circuit. The experimental goal of this chapter is to validate three different functioning models. The first model is a simple demonstration of the concept with a single dimensional array of electrodes. The second model expands upon the concept of the first, with a larger two-dimensional array of electrodes. The third is also a single dimensional array; however, it has a curved profile that resembles the shape of a finger tip. The third model is the first step towards one implementation of a 3D-printed tactical sensing prosthetic hand.

(a) Conceptual Design of Model

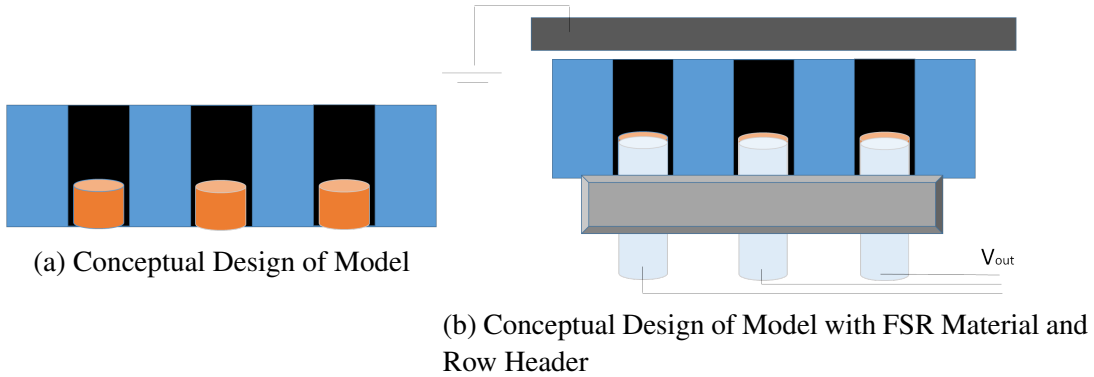(b) Conceptual Design of Model with FSR Material and Row Header

Figure 5.1: a: Cross-section of a model. The blue material is the normal PLA, the black material is the conductive plastic, and the orange material shows where the holes are printed into the conductive plastic. b: Cross-section of model with grounded FSR material on top and a row header connecting to the rest of the circuit on the bottom. The large black bar is the FSR, while the grey box with blue cylinders is the row header.

5.1 Design

Figure 5.1a shows a cross-section of a conceptual design for the printed model. Three electrodes with holes for connectors are printed in a 1D array. Figure 5.1b show the conceptual design of the sensor as a whole. An FSR material, described in detail in Chapter 2, is used for the pressure sensitive portion of the sensor. Due to the properties of the material, grounding a portion of the top side of the material will ground the entire surface. A row header is inserted in the bottom of the model to connect to the rest of the circuit.

The first sensor is a single set of three individual 3D-printed electrodes in a row with a flat surface. Figure 5.2a shows the CAD model for the first sensor. This sensor gives a simple demonstration to verify that the method for creating the sensors is done properly. Figure 5.2b shows a printed model of the 3×1 array. The printed
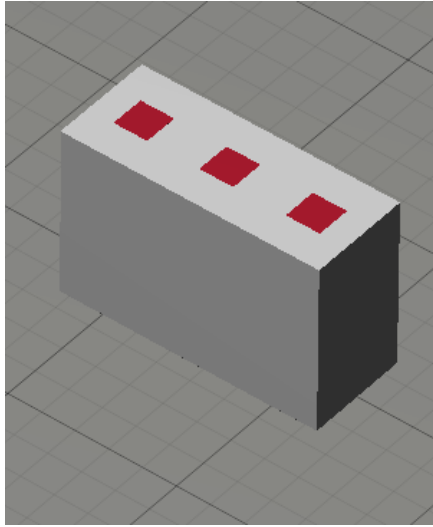
(a) 3×1 Array Model
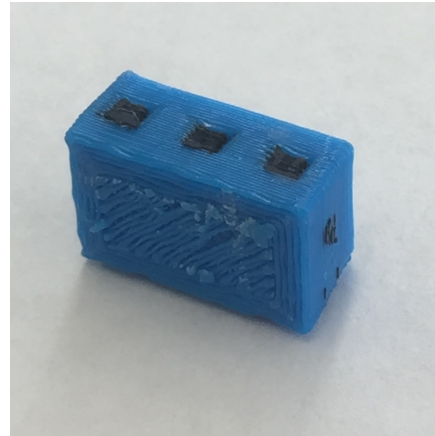
(b) 3×1 Array Print

Figure 5.2: a: CAD models for the 3×1 sensors. The red material is the conductive plastic, while the grey material is normal PLA. b: 3D-printed model. The black material is the conductive plastic, while the blue material is normal PLA.

model matches the desired shape and size of the CAD model, without any excess material or warped edges.

The sensors utilize many of the results from the previous chapters to simplify the design. The connectors from the printed conductor to the rest of the circuit are the same as those used in Chapter 4. The electrodes for each of the models are separated by a distance of 5.08 mm, or the minimum distance for a successful print, as determined in Chapter 4.

A 3D-printed cap is used to hold the FSR material in place. The cap is 0.4 mm larger than the dimensions of the sensor it is covering. Figure 5.3a shows a 3×1 array inserted into the circuit with a cap firmly in place.

Figure 5.3b shows the circuit diagram for the printed sensors. The circuit is a voltage divider. The 5 V and Ground come from the Arduino. The 3-D printed material is not a pressure sensor. R_{const} is the value of the constant resistor between

5 V and V_{out} in the circuit. The FSR material acts as variable resistors in the circuit, R_{var}. Pressure applied over one of the electrodes lowers the resistance of R_{var} and thus lowers V_{out}. To determine the value for R_{const}, the resistance of one electrode with the FSR material is measured with the probes of an ohmmeter. Resistance values are obtained for both minimal and maximum applied pressure which give values of R_{max} = 5 MΩ and R_{min} = 3.5 KΩ, respectively. The value of R_{const} that is chosen must satisfy the following relationship:

$$R_{min} << R_{const} << R_{max}. \tag{5.1}$$

R_{const} needs to be much larger than the R_{min} which is achieved when a large amount of pressure is applied to the FSR material lowering the resistance. R_{const} also needs to be much smaller than R_{max}, which is achieved when no contact is made with the sensors. When no contact is made with the sensor, V_{out} equals 5 V and R_{var} = R_{max} = 5 MΩ is much larger than R_{const}. In order to theoretically achieve a V_{out} of 0 V R_{var} = R_{min} =3.5 KΩ must be much smaller than R_{const}. Thus a value of 100KΩ between the two limits was chosen for R_{const}.
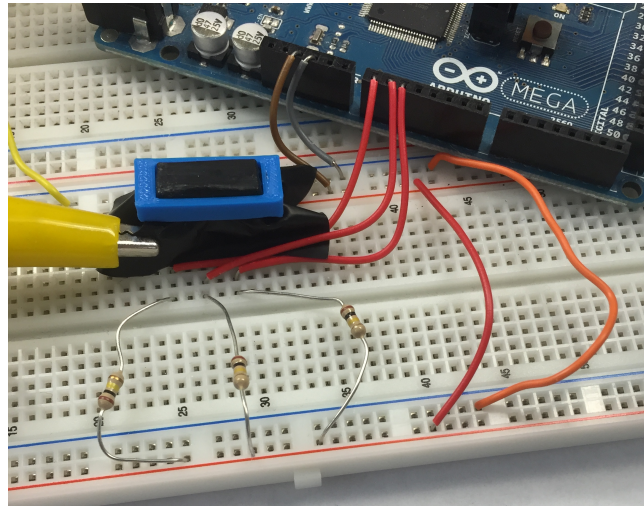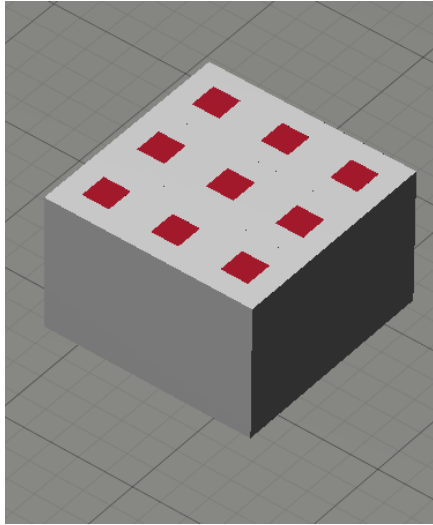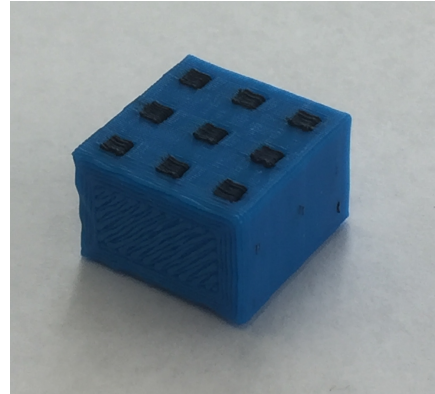
(a) Circuit
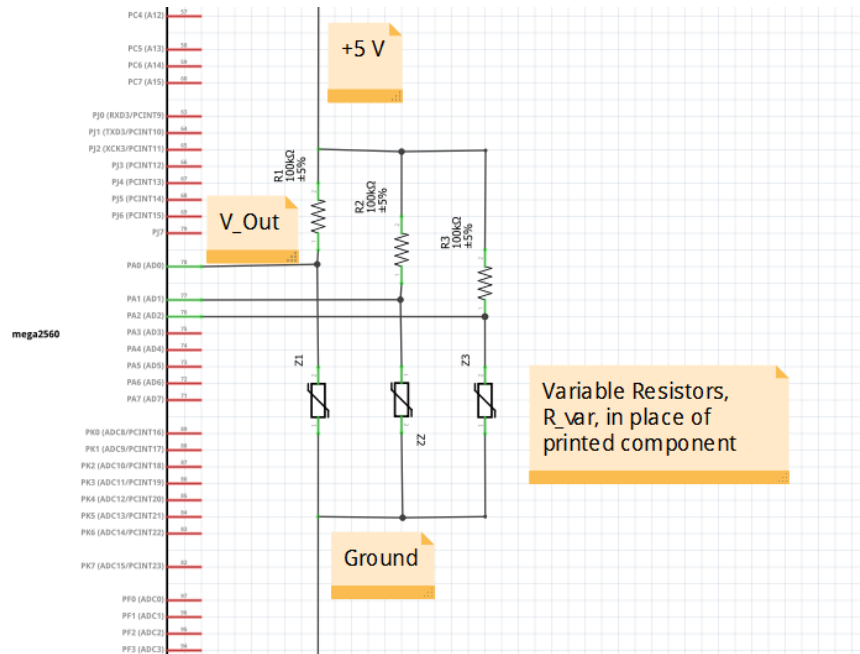
(b) Circuit Diagram

Figure 5.3: a: Circuit constructed on breadboard. b: Circuit diagram for 3×1 sensor.
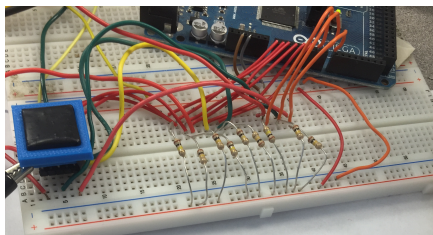
The second sensor consists of a 3×3 array of electrodes with a flat surface. Figure 5.4a and Figure 5.4b shows the CAD model and a printed model, respectively for the second sensor. A 3×3 array was chosen because it is a larger more complicated

(a) 3×3 Array Model
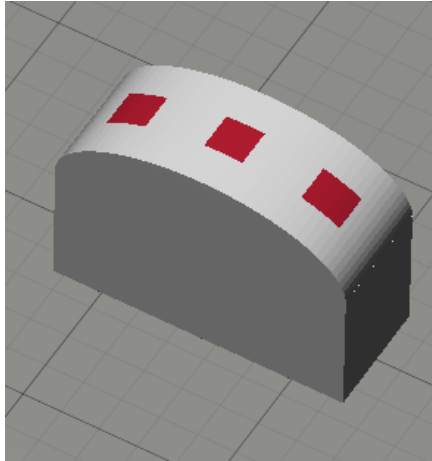

(b) 3×3 Array Print

(c) 3×3 Array Circuit

Figure 5.4: a: CAD model for the 3×3 sensor. The red material is the conductive plastic, while the grey material is normal PLA. b: 3×3 printed model. The black material is conductive plastic, while the blue is normal PLA. c: 3×3 senor inserted into circuit.

array. This sensor shows that the idea functions outside a simple case and paves the way for even larger arrays. Figure 5.4c shows the 3×3 sensor inserted into the circuit. The circuit diagram for this sensor is similar to that of the 3×1 array but has nine voltage dividers instead of three.

The third sensor is a more complex design. This sensor is closer in design to what would be used in a prosthetic limb. The third consists of a single set of three individual electrodes in a row with a rounded surface. Figure 5.5a and Figure 5.5b show the CAD model and a printed model, respectively for the third sensor. The

rounded surface is used as a rough approximation of the curve of a fingertip. The FSR material is modified for the rounded array. Two slits are cut in the sheet of FSR material used to cover the rounded array. The slits are there to help the material spread over the rounded surface more naturally. If the slits are not present, then the preloading on the FSR material renders the sensor inoperable. Without the slits in the FSR material, the noise level is too high to distinguish between activity and inactivity. The slits mitigate the preloaded pressure, but do not eliminate it entirely. Figure 5.5c shows the round sensor inserted into the circuit.

(a) Round Array Model

(b) Round Array Print
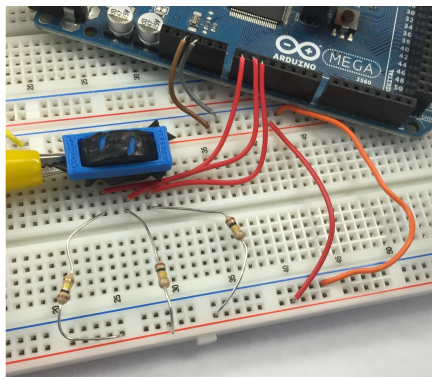
(c) Round Array Circuit

Figure 5.5: a: CAD models for the round sensor. The red material is the conductive plastic, while the grey material is normal PLA. b: Round printed model. The black material is conductive plastic, while the blue is normal PLA. c: Round senor inserted into circuit.

5.2 Senor Validation
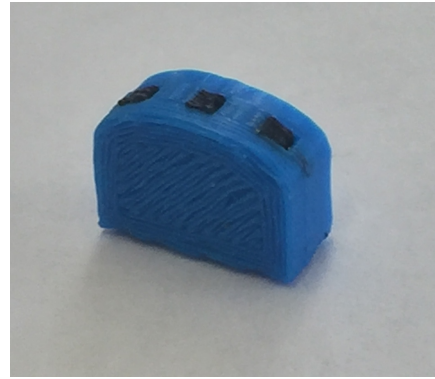
I conducted a number of tests for each of the sensors to verify their functionality. The first test is to find the range of values that the sensors can achieve. Ideally, there

should be little variance in the ranges for the three sensors. Second, a dowel rod is rolled across the top of each electrode in a sensor to find the voltage response over time. The dowel rods are rolled across in two configurations. First, the dowel rod is rolled flat against the top of the sensor, as depicted in Figure 5.6a. Second, the edge of the dowel rod is rolled at a 30° angle as illustrated in Figure 5.6b. Figure 5.6c and Figure 5.6d show how the electrodes are labeled for the 3×1 array and the 3×3 array, respectively. The 3×1 array and the round array use the same labels for the electrodes. The flat and angled experiments should be similar for the 3×1 array and the round array, but different for the 3×3 array. When the dowel rod is rolled flat across the top of the 3×3, array all of the sites in a column will be compressed at once, while the angled case will go over each electrode individually. For example, in the flat case the dowel rod is rolled over electrodes one, four, and seven at the same time, then moves on to two, five, and eight and so on.

There are two factors that are hypothesized to affect the voltage response of the sensors. The first is the surface area of contact between the grounding plane and the electrode. The second is the degree of compression of the FSR material. The surface area of contact is a large factor than the degree of compression. This observation is verified by using aluminum foil as the grounding plane. Using aluminum foil eliminates the piezoresistive factor or the degree of compression. The voltage response when using aluminum foil is similar to that of the FSR material.
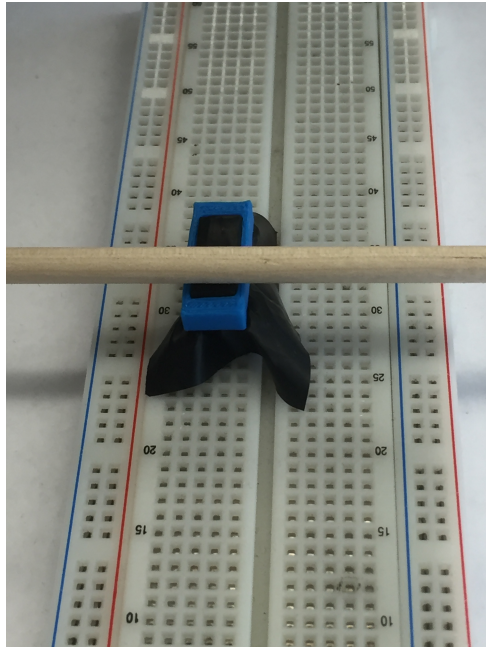
(a) Flat Dowel Rod
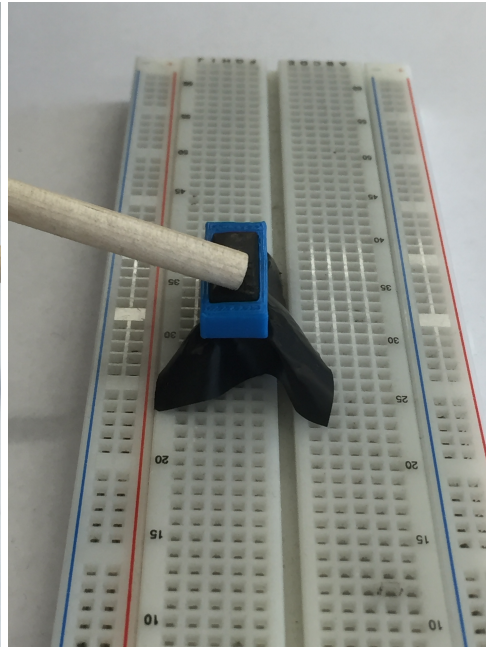
(b) Angled Dowel Rod
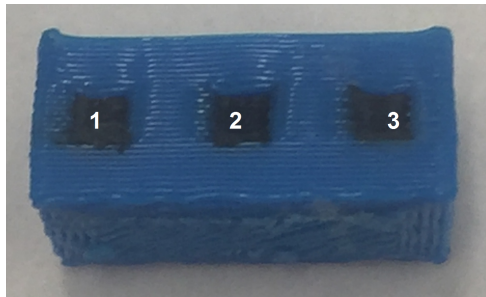
(c) 3×1 and Round Array Electrode Configuration

(d) 3×3 Array Electrode Configuration

Figure 5.6: (a) and (b) The dowel rod is rolled across the top of the sensor. (c) The labels applied to the electrodes for the 3×1 Array and the Round Array (d) The labels applied to the electrodes for the 3×3 Array
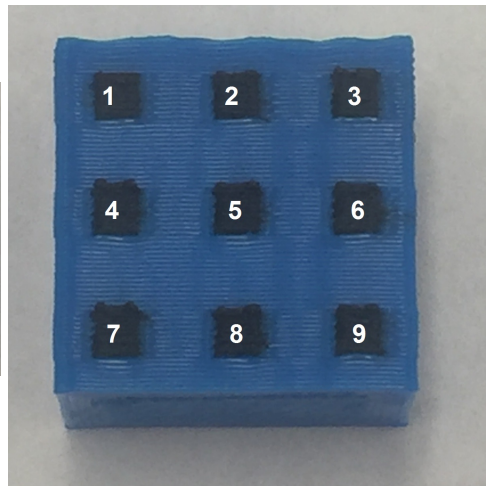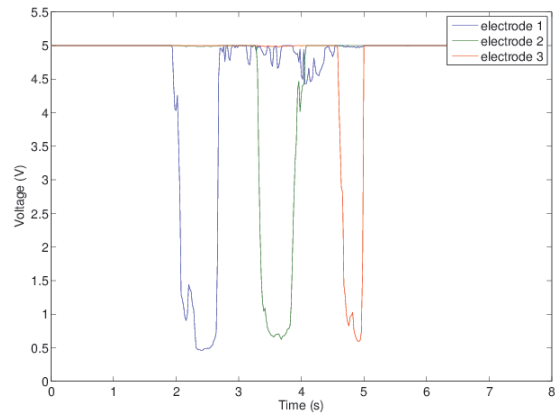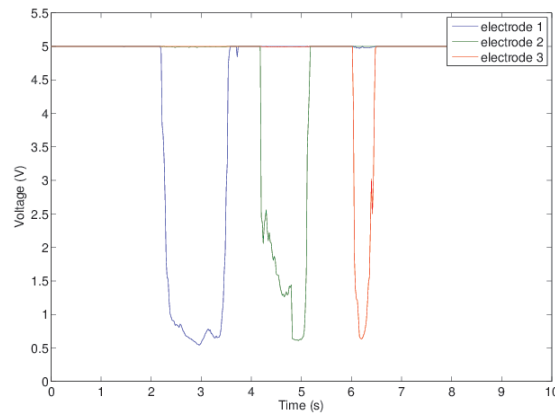
5.2.1 3×1 **Array**

The voltages range for the 3×1 array was between 0.54 V and 5 V. Figure 5.7a and Figure 5.7b show the voltage response for the flat and angled cases, respectively. The dowel rod starts on the left with the first electrode and rolls to the right. Each electrode is only active when the dowel rod compresses the FSR material over the printed conductive material. The voltage response of the sensor shows that it functions as expected. For the flat case, electrodes one, two, and three are active between two and three seconds, three and four seconds, and four and a half to five and a half seconds, respectively. There is a slight amount of noise three and five seconds where the action of pulling the dowel rod across the face of the sensor causes contact between the FSR material and the first electrode. However, the noise is very slight voltage response of the activation. In the angled case, electrodes one, two, and three are active between two and three and a half seconds, four and five and a half seconds, and six and seven seconds. The noise that was present in the flat case is largely absent in this case. The difference comes from the way the dowel rod is rolled across the surface. The 3×1 array is a baseline to compare against the other two sensors.

(a) Flat Dowel Rod

(b) Angled Dowel Rod

Figure 5.7: Voltage Response as a function of time for 3×1 Array. Blue is electrode 1, or the electrode on the left. Green is electrode 2, or the middle electrode. Red is electrode 3, or the electrode on the right.

5.2.2 3×3 Array

The range for the 3×3 array is from 1.03 V and 5 V. Figure 5.8a and Figure 5.8b show the voltage response for the flat and angled cases, respectively. During the

testing, it was found that the surface of the array is slightly warped. The center portion is slightly lower than the rest of the sensor. The cavity caused some error with the rigid dowel rod where pressure was not evenly applied and thus electrodes one, four, and six should have been more active had a lower response. The lower activation is seen in the flat case around one second for electrodes one and four and around five second for electrode six. The second set of electrodes, two, five, and eight are activated around three second. The third set of electrodes, three, six, and nine are activated around five seconds. The angled case performed well, showing activation only when the dowel rod was over an electrode. The pattern is similar to that used with the other two arrays. One row is activated at a time. However, in this case there are two additional rows of electrodes.
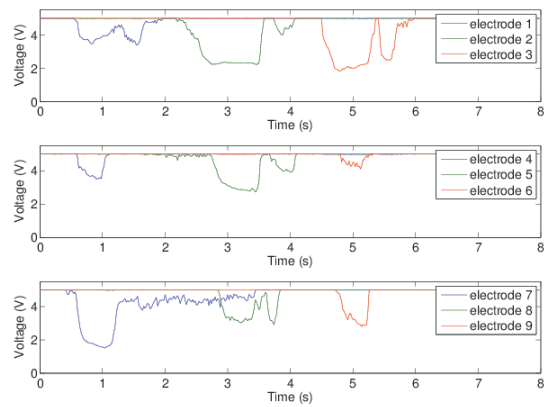
(a) Flat Dowel Rod
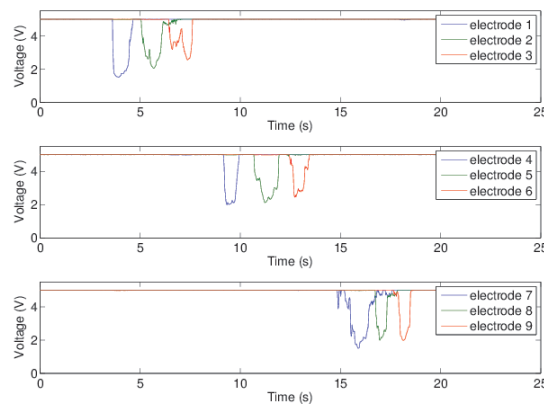
(b) Angled Dowel Rod

Figure 5.8: Voltage Response as a function of time for 3×3 Array. Blue is electrodes 1, 4, and 7, or the left set of electrodes. Green is electrodes 2, 5, and 8, or the middle set of electrodes. Red is electrode 3, 6, and 9, or the right set of electrodes.

5.2.3 Rounded Array

The rounded array had two sets of voltage ranges. The first is the unloaded case. This case is classified as the unloaded because is this case the cap rest lightly on top

of the model. In this configuration the cap does not add any preloaded pressure to the sensor. The voltage range, 0.88 V to 5.0 V, is similar to the other two sensors. The second case is the preloaded case. In this case, the cap is secured firmly in place, similar to how the cap is for the previous two sensors. The voltage range, 0.88 V to 3.91 V, is lower because the cap creates preloaded pressure on the sensor. A calibration process could be undertaken to correct for this bias. However, the calibration would have to be done for the other cases, as well.
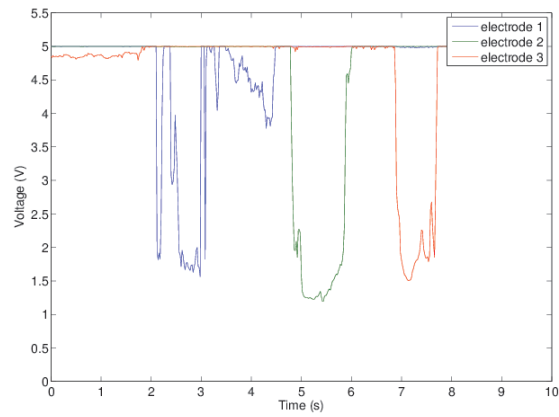
Figure 5.9 shows the voltage response for the unloaded case. For the flat case, electrodes one, two and three are active from approximately one second two seconds, two seconds to four seconds, and four and a half second to five and half seconds, respectively. For the angled case, electrodes one, two and three are active from approximately two seconds and three seconds, five seconds and six seconds, and seven seconds and eight seconds, respectively. The response shows activation at an electrode only when the dowel rod is rolled over. The voltage responses, in the unloaded cases, are lower than that of the 3×3 array. A possible explanation for the lower response is the difference in rolling a dowel rod across a flat surface versus a rounded surface. Rolling a dowel rod across a rounded surface is more difficult than a flat surface. The amount of pressure one can apply is less for a rounded surface, especially on the downward slope. If pressure is applied in the wrong direction, then the dowel rod will slip off the surface giving poor results.

Figure 5.10 shows the voltage response for the preloaded cases. Even though the range is smaller, the sensor still functions essentially the same as the flat array. For the flat case, electrodes one, two, and three are active from approximately three second to

four and a half seconds, five and a half seconds and seven seconds, and eight seconds and nine seconds, respectively. For the angled case the electrodes one, two, and three are active from approximately two seconds and six seconds, seven seconds and nine seconds, and eleven second to thirteen seconds, respectively. Only the electrode that the dowel rod is over shows activation on the voltage response. At some points, the voltage for one of the inactive sensors jumps up to 5.0 V. This phenomenon occurs when the motion of the dowel rod causes separation between the FSR material and the electrode creating an infinite resistance. The angled case has less occurrences of the phenomenon because there is less tension on the FSR material as the dowel rod is rolled across. The reduction in tension means that the dowel rod has a lesser effect on the rest of the FSR material. Data was collected a second time for the flat case, the results of which can be seen in Figure 5.10c. For the second flat case, electrodes one, two, and three are active from approximately three seconds to five seconds, six seconds to eight seconds, and nine seconds to ten seconds, respectively. In this case, the FSR material separates less from the electrodes.
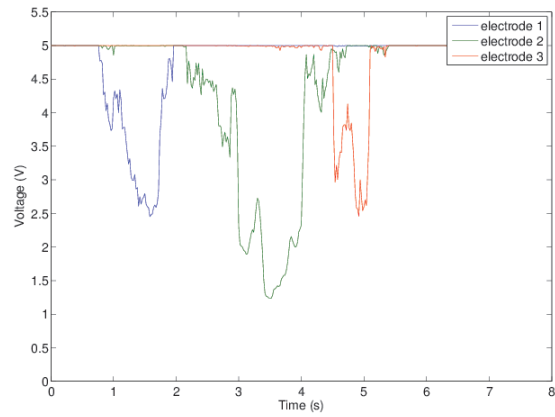
(a) Flat Dowel Rod

(b) Angled Dowel Rod

Figure 5.9: Voltage Response as a function of time for the unloaded cases. Blue is electrode 1, or the electrode on the left. Green is electrode 2, or the middle electrode. Red is electrode 3, or the electrode on the right.
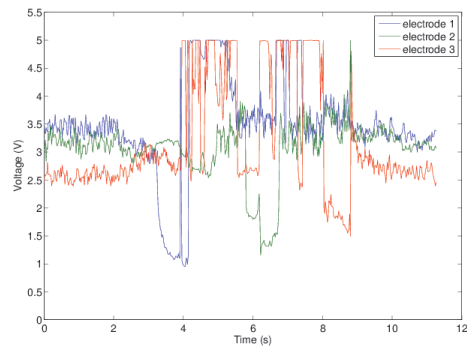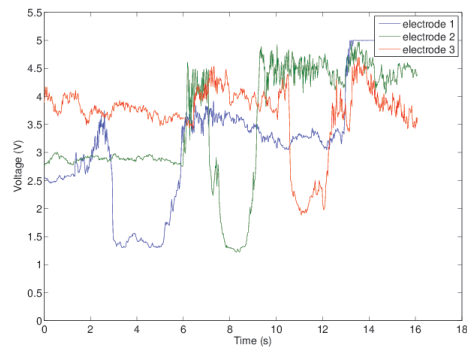
(a) Flat Dowel Rod

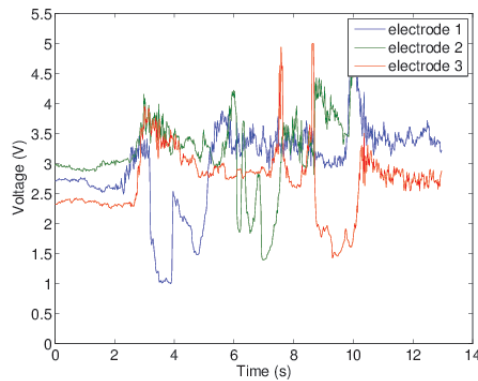
(b) Angled Dowel Rod

(c) Second Flat Dowel Rod

Figure 5.10: Voltage Response as a function of time for the preloaded cases. Blue is electrode 1, or the electrode on the left. Green is electrode 2, or the middle electrode. Red is electrode 3, or the electrode on the right.

5.3 Discussion

The results from the various experiments show that the 3D printed pressure sensors generally function as expected. The 3×3 array demonstrates that the process can be expanded to larger systems involving more electrodes. The rounded case shows the versatility of the 3D printer. A combined 3×3 rounded tip array would be the next step towards a 3D printed tactile sensing prosthetic hand.

There are a number of ways improvements could be made to the design. Several errors originated from the fact that a single sheet of FSR material is used for the entire sensor. It would be possible to mechanically separate the FSR material for each electrode or a group of smaller electrodes in a larger array. Separating the FSR material would isolate the electrodes. Isolating the electrodes would ensure that crosstalk does not occur. Crosstalk is where activation at one electrode adversely affects a different electrode. Another concern is that currently a single analog input is required for each electrode. The required analog inputs for larger arrays can become a significant problem. Multiplexing is one solution, which can be added to reduce the required number of analog inputs. Using the current analog inputs, a frequency-divisor multiplexor would be used. In frequency-divisor multiplexing the spectrum of each inputs are shifted to their own unique frequency. Furthermore, the circuit can be designed for time-division multiplexing so that there is local conversion at the finger that is then transmitted digitally back to the central processing unit. In time-division multiplexing the inputs are separated by a delay in time.

Chapter 6

Conclusions

3D-printing has been leveraged in many fields to increase customization and reduce cost. The introduction of conductive filament allows circuits to be designed and printed. Producers of prostheses have already utilized the 3D-printing to allow a larger portion of the population to have access to prosthetic limbs. The use of conductive filaments could make 3D-printed sensing prostheses more readily available, as well. A sensing prosthesis would restore not only the function of having a limb but also the sensations that go along with it.

In this thesis, I have verified the functionality of the F-Electric ™ material through several experiments. I integrated the F-Electric ™ with nonconductive PLA to make a simple circuit built into the physical structure. During this portion of the research, I developed some practices that help to optimize print success with the Makerbot Replicator 2X ™. I also established ways to connect the printed electrodes with an outside circuit successfully. Finally, I utilized the conductive material to create the circuitry for three partially 3D-printed pressure sensors. The sensors function overall

as expected. The round sensor that matches the profile of a finger is a step towards one implementation of a 3D-printed tactile sensing prosthetic hand.

There are several directions the project can be taken in the future. Larger array networks can be designed and implemented. A larger network would allow for a greater resolution to touch sensitivity. Introducing larger networks would also add to the complexity of the circuitry needed. The current setup requires an analog input for every node. Using a multiplexing system to string an entire row of nodes together would reduce the number of needed inputs.

The current designs of the components are optimized for use with a breadboard. In addition, the current designs are fairly simplistic in nature and do not make full use of the capabilities of 3D-printing.

Integration with prosthetics is the end goal of this project. The research done has shown that 3D-printed wiring for a tactile-sensor is possible. Next steps in the research can be integrating more sophisticated systems with the 3D-printed components.

Bibliography

Alexander, B. and Viktor, K. (2010). Proportions of hand segments. *International Journal of Morphology*, 28(3):755–758.

Biddiss, E. A. and Chau, T. T. (2007). Upper limb prosthesis use and abandonment: A survey of the last 25 years. *Prosthetics and Orthotics International*, 31(3):236–257.

Buehler, E., Branham, S., Ali, A., Chang, J. J., Hofmann, M. K., Hurst, A., and Kane, S. K. (2015). Sharing is caring: Assistive technology designs on thingiverse. In *Proceedings of the 33rd Annual ACM Conference on Human Factors in Computing Systems*, CHI '15, pages 525–534, New York, NY, USA. ACM.

Chilson, L. (2013). The difference between ABS and PLA for 3D printing. *URL: http://www.protoparadigm.com/news-updates/the-difference-between-abs-and-pla-for-3d-printing*. [Accessed: March 2016].

Clippinger, F. W., Avery, R., and Titus, B. R. (1974). A sensory feedback system for an upper-limb amputation prosthesis. *Bulletin of prosthetics research*, pages 247 – 258.

Cram, D., Dick, A., and Cram, A. (2015). Conductive PLA. https://www.proto-pasta.com/pages/conductive-pla [Accessed: March 2016].

Ekman, A. (2016). Regaining sense of touch: Artificial, pressure-sensitive skin for hand prosthetics. *Lund University*. Student Paper. https://lup.lub.lu.se/student-papers/search/publication/8596987[Accessed: July 2016].

English, A. R. (2012). 3D Printer Filament Buyer's Guide. *URL: http://www.protoparadigm.com/news-updates/3d-printer-filament-buyers-guide/*. [Accessed: March 2016].

Feygin, M. and Pak, S. (1999). Laminated object manufacturing apparatus and method. US Patent 5,876,550.

Gibbard, J. (2013). Open hand project. `http://www.openhandproject.org/index.php`. [Accessed: March 2016].

Gross, B. C., Erkal, J. L., Lockwood, S. Y., Chen, C., and Spence, D. M. (2014). Evaluation of 3D printing and its potential impact on biotechnology and the chemical sciences. *Analytical Chemistry*, 86(7):3240–3253. PMID: 24432804.

Grout, P. and Truesdell, J. (2014). A helping hand for a freind. *People*, 81(10):8283.

Hammond, F. L., Meng, Y., and Wood, R. J. (2014). Toward a modular soft sensor-embedded glove for human hand motion and tactile pressure measurement. In *the 2014 IEEE/RSJ International Conference on Intelligent Robots and Systems (IROS 2014)*, pages 4000–4007.

Hübler, A., Schmidt, G., Kempa, H., Reuter, K., Hambsch, M., and Bellmann, M. (2011). Three-dimensional integrated circuit using printed electronics. *Organic Electronics*, 12(3):419 – 423.

Hull, C. (1986). Apparatus for production of three-dimensional objects by stereolithography. US Patent 4,575,330.

Hurst, A. and Tobias, J. (2011). Empowering individuals with do-it-yourself assistive technology. In *The Proceedings of the 13th International ACM SIGACCESS Conference on Computers and Accessibility*, ASSETS '11, pages 11–18, New York, NY, USA. ACM.

Leigh, S. J., Bradley, R. J., Purssell, C. P., Billson, D. R., and Hutchins, D. A. (2012). A simple, low-cost conductive composite material for 3D printing of electronic sensors. *PLoS ONE*, 7(11):1–6.

Mohney, G. (2013). Health care cost for boston marathon amputees add up over time. `http://abcnews.go.com/Health/health-care-costs-boston-marathon-amputees-add-time/story?id=19035114/`[Accessed: March 2016].

Nouchi, R., Saito, T., and Tanigaki, K. (2012). Observation of negative contact resistances in graphene field-effect transistors. *Journal of Applied Physics*, 111(8):084314–084314.

Novakova-Marcincinova, L., Novak-Marcincin, J., Barna, J., and Torok, J. (2012). Special materials used in fdm rapid prototyping technology application. In *2012 IEEE 16th International Conference on Intelligent Engineering Systems (INES)*, pages 73–76.

Raspopovic, S., Capogrosso, M., Petrini, F. M., Bonizzato, M., Rigosa, J., Di Pino, G., Carpaneto, J., Controzzi, M., Boretius, T., Fernandez, E., Granata, G., Oddo, C. M., Citi, L., Ciancio, A. L., Cipriani, C., Carrozza, M. C., Jensen, W., Guglielmelli, E., Stieglitz, T., Rossini, P. M., and Micera, S. (2014). Restoring natural sensory feedback in real-time bidirectional hand prostheses. *Science Translational Medicine*, 6(222):222ra19–222ra19.

Resnik, L., Klinger, S. L., and Etter, K. (2014). The DEKA Arm: Its features, functionality, and evolution during the Veterans Affairs Study to optimize the DEKA Arm. *Prosthetics and Orthotics International*, 38(6):492–504.

Shemelya, C., Banuelos-Chacon, L., Melendez, A., Kief, C., Espalin, D., Wicker, R., Krijnen, G., and MacDonald, E. (2015a). Multi-functional 3D printed and embedded sensors for satellite qualification structures. In *SENSORS, 2015 IEEE*, pages 1–4. 10.1109/ICSENS.2015.7370541.

Shemelya, C., Cedillos, F., Aguilera, E., Espalin, D., Muse, D., Wicker, R., and MacDonald, E. (2015b). Encapsulated copper wire and copper mesh capacitive sensing for 3-D printing applications. *IEEE Sensors Journal*, 15(2):1280–1286.

Shemelya, C., Cedillos, F., Aguilera, E., Maestas, E., Ramos, J., Espalin, D., Muse, D., Wicker, R., and MacDonald, E. (2013). 3D printed capacitive sensors. In *SENSORS, 2013 IEEE*, pages 1–4. 10.1109/ICSENS.2013.6688247.

Tan, D. W., Schiefer, M. A., Keith, M. W., Anderson, J. R., Tyler, J., and Tyler, D. J. (2014). A neural interface provides long-term stable natural touch perception. *Science translational medicine*, 6(257):257ra138–257ra138.

Toutonghi, M. (2015). Tips and designs for 3D printing electronics with F-Electric. `http://functionalize.com/tips-and-designs-for-3d-printing-electronics-with-conductive-filament/`[Accessed: March 2016].

Velez, M. (2014). Dad uses 3D printer to make his son a prosthetic hand (video). *The Huffington Post*. `http://www.huffingtonpost.com/2013/11/04/dad-prints-prosthetic-hand-leon-mccarthy_n_4214217.html` [Accessed: March 2016].